



OPEN

Spatiotemporal effects of landscape structure on the trade-offs and synergies among ecosystem service functions in Yangtze River Economic Belt, China

Yao Yao¹ & Yuanyuan Yang^{2,3}✉

Effective landscape management is vital for maximizing the availability of ecosystem service functions (ESF). However, how landscape pattern simultaneously affects multiple ESF across time and space, specifically regarding changes in their relationships, has not been comprehensively evaluated. Accordingly, the current study examines the dynamic impact of landscape pattern on the interactions among ESF trade-offs in China's Yangtze River Economic Belt (YREB) from 1990 to 2020. Five key ESF are evaluated: carbon sequestration (CS), food supply (FS), habitat quality (HQ), water retention (WR), and soil conservation (SC). The geographical and temporal weighted regression model is adopted to analyze how these relationships are influenced by changes in the landscape pattern over 30 years. Over the past three decades, the overall amounts of FS, WR, and SC have increased, with only WR exhibiting a sustained increasing trend, while CS and HQ have significantly decreased. The trade-off coordination effects among the ESF generally transitioned from trade-offs to synergies, with the CS-FS change more pronounced, shifting from weak trade-offs (-0.29) to synergies (0.20). Significant spatial variations were also observed. Most landscape pattern significantly impact the relationships among ESF. Specifically, landscape composition has a stronger influence on ecosystems than configuration; however, these effects are diverse and often inconsistent, requiring decision-makers to continuously balance landscape management. The impacts of landscape pattern on the relationships between SC and other ESF (CS-SC, HQ-SC, HQ-SC, and WR-SC) were consistent, with the most prominent impact on CS-SC. This suggests that landscape pattern exerts a comparatively steady impact on CS, benefiting from the contributions of decision-makers to soil conservation in regional land parcels. These results underscore the intricate responses of inter-ecosystem relationships to landscape pattern and the need for dynamic trade-offs in landscape management. Cumulatively, this study provides crucial guidance for policymakers in designing effective landscape management policies to mitigate ecological degradation.

Keywords Ecosystem service functions, Landscape pattern, Trade-off, Synergy, Sustainable landscape management, Yangtze River Economic Belt

Various ecosystem service functions (ESF) are directly linked to human survival and development, serving as important interfaces between humanity and the environment^{1–3}. With the growing global population and accelerated urbanization, the demand for land resource development is becoming increasingly evident^{4–7}. These developments have spurred marked alterations to the landscape and precipitated myriad adverse ecological ramifications, including reduced ESF and soil erosion, among others^{8–10}. Recently, evaluating how human activities alter landscape pattern and their impact on the balance between ecosystems has garnered increased research attention^{11–13}. Landscape ecology aims to elucidate the spatial patterns and ecological processes in a reciprocal relationship^{14–16}. Therefore, landscape pattern is a significant indicator of landscape heterogeneity and affects multiple ecological processes^{17,18}. Additionally, structural and functional interactions between ESF

¹School of Public Management, Guizhou University of Finance and Economics, Guiyang 500025, China. ²School of Tourism Management, Guizhou University of Commerce, Guiyang 550014, China. ³School of Public Administration, China University of Geosciences, Wuhan 430074, China. ✉email: 739271126@qq.com

often determine tradeoffs and collaborations^{19–21}. The interplay among ESF significantly promotes sustainable management of ecosystems and effective resource distribution^{22,23}. Scenarios are created by combining landscape layout, crops, and the resulting service compromises, where ESF can be harmonized or in conflict^{24–26}. Hence, to present a credible case for sustainable production policies, the influence of landscape design on the cooperative equilibrium of ESF must be characterized^{27–29}.

ESF denote the natural environmental conditions and benefits upon which humanity relies for the survival, formation, and sustainability of ecosystems^{30,31}. This encompasses every advantage that humans gain directly or indirectly from ecosystems^{32,33}. Due to their diverse range, the spatial distribution of ESF is uneven with selective human utilization. Thus, the relationships among ESF exhibit dynamic changes, manifesting as trade-offs and synergies^{34,35}. Tradeoffs occur when the provision of certain ESF decreases as the use of others increases; in contrast, synergies refer to the simultaneous enhancement of two or more environmental management mechanisms^{36–39}. As the understanding of the tradeoffs and synergies of ESF has deepened, analyses have transitioned from individualistic to collaborative associative^{40,41}. Research has primarily focused on internal trade-offs and synergies in ecosystems and between ecosystems and other systems^{36,42,43}. ESF are significantly influenced by climatic factors, including precipitation and temperature, whereas land-use changes associated with human activities are considered the most prominent, significant, and direct driving forces^{44,45}. Landscape pattern refers to the configuration of land use and land cover (LULC). ESF are affected by the landscape composition and layout^{46–48}. However, often, when evaluating the environmental impacts of landscape pattern on ESF, only the influences of individual ecological indicators are considered while disregarding the internal impacts between ecosystems^{49–52}. For example, a study on how landscape design influences ES value between 2000 and 2018 revealed that the landscape pattern has markedly impacted the ESF within the Central Plains Urban Agglomeration (CPUA)⁴⁹. Moreover, studies investigating the spatiotemporal dynamics and impacts of landscape pattern on ESF over an extended time series are scarce.

The Yangtze River Economic Belt (YREB) is rich in environmental and elemental resources^{46,53}. The YREB is demonstrably undergoing rapid economic and social transformation^{54,55}. With the progression of modern urbanization and projects such as the Belt and Road Initiative, the YREB is set to transform into a crucial area for facilitating the movement of populations and industries within China. However, the prolonged and rapid urbanization process exacerbates unsustainable land utilization, posing several challenges to the ecological environment, including poor overall phenomena, a dwindling ecosystem, and deteriorated service functions^{56,57}. As a pivotal region for China's ecological security and coordinated economic development, the YREB offers an irreplaceable research context for unraveling human–environment interaction mechanisms and advancing sustainable development strategies. Its profound transformations in landscape pattern and marked degradation/recovery processes of ESs provide critical insights. Research in this region may serve as a theoretical and practical paradigm for global river basins grappling with the tension between rapid urbanization and ecological conservation.

The primary objective of the current study is to evaluate the dynamic impact of landscape pattern on the interactions among ES trade-offs by incorporating two types of synergies at various temporal and spatial scales, contingent on the spatiotemporal diversity of influencing elements. Ultimately, this study seeks to enhance the effectiveness of ecological and environmental safeguards in the YERB, offering critical insights to guide superior quality development.

Material and methods

The water resources in the YERB were divided into 476 hydrological basins; the dispersion traits of five representative hydrological basins (carbon sequestration (CS), food supply (FS), habitat quality (HQ), water retention (WR), and soil conservation (SC)) were assessed from 1990 to 2020. Furthermore, the Geographical and Temporal Weighted Regression (GTWR) model was adopted to investigate interaction models between landscape structure and the trade-offs and synergies among ESF (TS–ESF).

Study site

The YREB, in the Yangtze River Basin (YRB), is an essential connection and vital economic area for China's development. Despite covering only one-fifth of the country's land area, it supports over one-third of the population and the national Gross Domestic Product (GDP), occupying an influential position in China's pursuit of high-quality economic growth. By 2020, the YREB's GDP had increased to 47.2 trillion yuan, with a population of 606 million, accounting for 46.4% and 42.9% of the total GDP and population, respectively. In fact, the three primary economic regions in eastern, central, and western China comprise the YREB (Fig. 1). YREB includes 11 provinces, including mountains, hills, plains, wetlands and other landforms, the overall elevation gradient from west to east, forming a three-tier ladder, landscape types are rich. In addition, from the perspective of ESF, the entire YREB can be divided into water and soil conservation areas in the upper reaches, lake wetland groups in the middle reaches, and estuary deltas in the lower reaches. However, this is a region with rapid economic development in China, and the accelerated process of urbanization and industrialization may lead to drastic changes in landscape pattern, such as urban expansion, changes in agricultural land, and construction of industrial zones. These changes can have considerable impacts on ecosystem services, such as increased soil erosion, reduced water quality, and reduced biodiversity. Therefore, the study of the relationship between landscape structure and ESF here can provide references for sustainable development and balance economic development and ecological protection.

Data sources and preprocessing

This research employed watershed boundaries, land use and land cover (LULC) data, a digital model of elevation (DEM), the normalized difference vegetation index (NDVI), weather-related data, crop reference

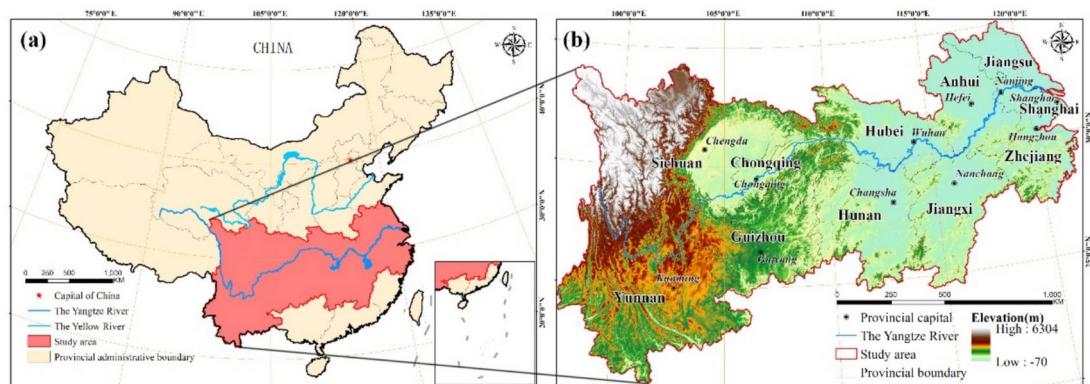


Fig. 1. Administrative districts of the YREB. Location of the YREB in China (a), The administrative districts of the YREB (b). Regional division: The upstream region includes Chongqing Municipality, Sichuan Province, Guizhou Province and Yunnan Province; the middle region includes Jiangxi Province, Hunan Province and Hubei Province; the downstream region includes Anhui Province, Shanghai City, Jiangsu Province and Zhejiang Province (b). Maps were drawn by authors, using ArcGIS 10.8 (Environmental Systems Research Institute, USA. <https://www.esri.com/>).

Data type	Data format	Spatial resolution	Time	Data source/processing
Administrative boundaries	Shapefile/polygon	–	2020	Data Center for Resources and Environmental Sciences, Chinese Academy of Sciences (http://www.resdc.cn)
Land use and land cover (LULC)	Raster	1 km	1990–2020	
Digital elevation model (DEM)	Raster	1 km	2020	
Normalized difference vegetation index (NDVI)	Raster	1 km	1990–2020	
Catchment boundaries	Shapefile/polygon	–	–	
Meteorological data	Shapefile/point	–	1990–2020	HydroSHEDS dataset (https://hydrosheds.org)
Crop reference evapotranspiration (CRE)	Shapefile/point	–	1990–2020	China Meteorological Data Service Centre (http://data.cma.cn)
World soil data set	Raster	1 km	2000	National Earth System Science Data Center (http://data.cma.cn)
Socioeconomic data	Spreadsheet	–	1990–2020	National cryosphere Desert Data Center (https://www.crensed.ac.cn/portal)
				Statistical Yearbook of Provinces and Cities in the YREB

Table 1. Dataset details and sources employed in this study.

evapotranspiration (CRE) data, the World Soil Data Set, and socioeconomic information (Table 1). Moreover, spatial data was converted to a uniform coordinate system with a spatial resolution of $1\text{ km} \times 1\text{ km}$. Moreover, all the indices at the landscape class level (PD, PLAND, and AREA_MN) were associated with agricultural land, encompassing farmland, woodland, and grassland, i.e., the three land use categories.

Methods

The workflow for this study is depicted in Fig. 2. Initially, 476 hydrological basin units were developed for cartographic and analytical purposes, using the HydroSHEDS dataset as a basis. Due to their association with numerous ecological processes, catchments were deemed appropriate units for this study^{58–60}. A proximate elevated watershed was incorporated into a partial watershed zone on the fringe of the area (typically $< 1\text{ km}^2$). Subsequently, an ESF assessment was performed, trade-off and synergy relationships were identified (see "Ecosystem service functions assessment and identification of trade-off and synergy relationships"), and the landscape pattern was quantified (see "Quantification of landscape pattern"). The number of basins in 1990, 2000, 2010, and 2020 was determined. Ultimately, the landscape pattern and TS-ESF served as explanatory and predictive factors in the local regression models, respectively. These models were employed to examine the effects of altered landscape pattern on ten distinct TS-ESF (see "Interactions between landscape formation and the compromises and cooperative effects among ecosystem service functions, as identified via GTWR").

Ecosystem service functions assessment and identification of trade-off and synergy relationships

The ES system was assessed. Considering the true circumstances of the YREB and data availability, five representative ESF, namely CS, FS, HQ, WR, and SC, were ultimately selected. FS utilized the NDVI and LULC data in the spatial allocation evaluation, while other ESF employed the "Integrated Assessment of ESF and Trade-offs" (InVEST) system. Table 2 presents detailed information on the models and data used for each service; the specific calculations are presented in Appendix B. The spatial analysis tools in ArcGIS 10.8 were used to quantify each service (ESRI, United States)^{61,62}.

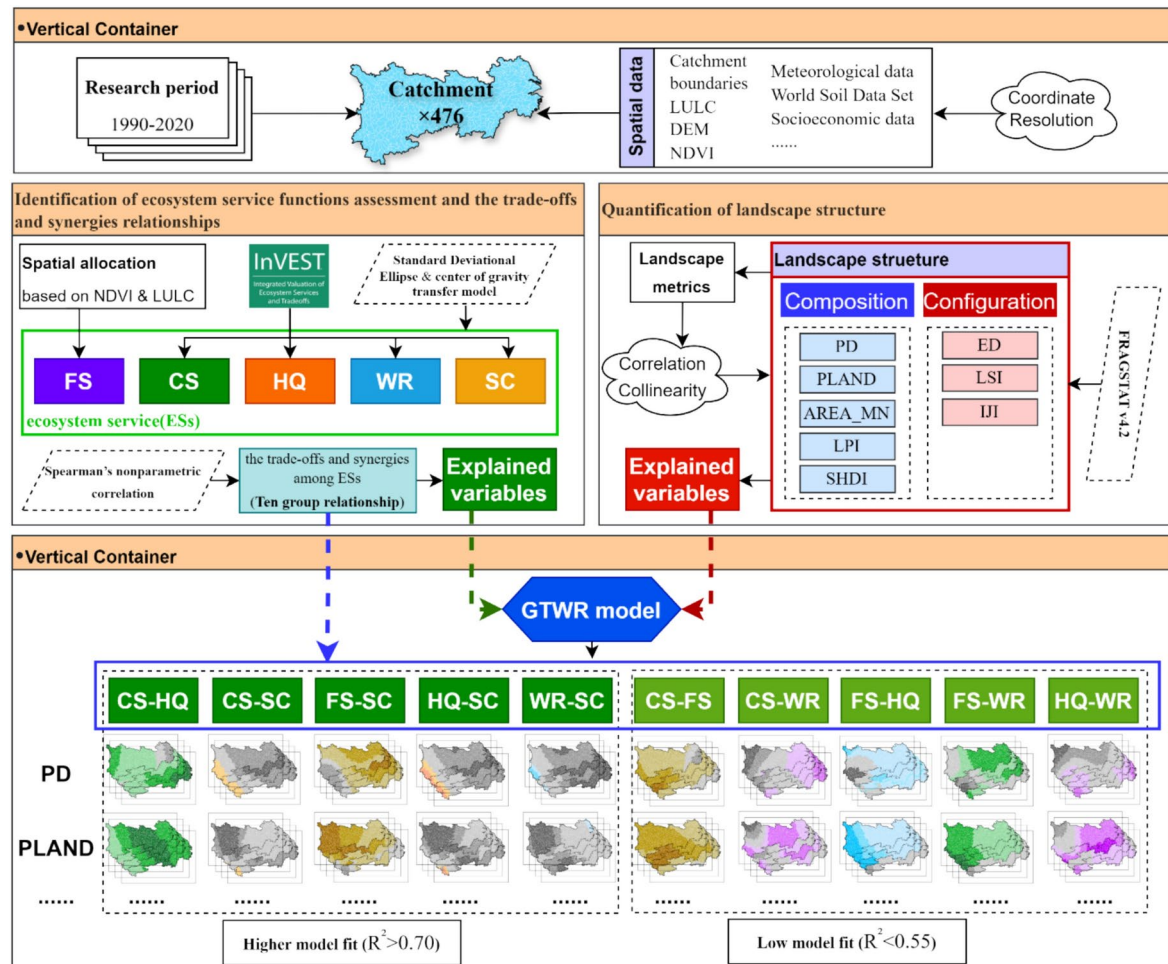


Fig. 2. Illustration of the correlation between landscape pattern and TS-ESF. CS carbon sequestration, FS food supply, HQ habitat quality, WR water retention, and SC soil conservation. Maps were drawn by authors, using ArcGIS 10.8 (Environmental Systems Research Institute, USA. <https://www.esri.com/>).

Ecosystem service functions	Unit	Methodology	Data required
Carbon storage (CS)	t/ha	InVEST carbon storage and sequestration model	LULC, NDVI, and the carbon stock parameters
Food production (FP)	t/ha	Strong linear relationship between NDVI and crop yield	NDVI, total food production
Water conservation (WC)	m ³ /ha	InVEST water yield model	DEM, LULC, meteorological information, soil information and empirical parameters
Soil conservation (SC)	t/ha	InVEST soil conservation model	DEM, LULC, NDVI, meteorological information, soil information and empirical parameters
Habitat quality (HQ)	-	InVEST-HQ	LULC, threat and sensitivity data

Table 2. Ecosystem service functions definitions and calculations.

The standard deviational ellipse (SDE) and Center of Gravity Transfer Model (COGM) were utilized to elucidate the developmental features and patterns of ESF between 1990 and 2020. The SDE quantitatively explains the centrality, dispersion, directionality, spatial morphology, and other characteristics of the geographic feature distribution from global and spatial perspectives^{63–65}. COGM, as a key indicator, accurately maps the distribution characteristics of various geographical features in an ES system in time and space. Furthermore, the direction and distance of gravity movement reveal the degree of change and spatial differences in the geographical features of the ESF system over a specific period. To intuitively track this trajectory of gravity migration and interpret the underlying changes, the MeanCenter function in ArcGIS software was combined with actual conditions to perform a thorough analysis of the trends^{66–68}.

A nonparametric Spearman's rank correlation analysis was performed at the watershed spatial scale in 1990, 2000, 2010, and 2020 using the "corrplot" via the package in R 4.0 software to evaluate the compromises

and synergies between different ESF. This method is widely used to quantify and determine the directions and strengths of these relationships^{69–71}. Positive and negative correlations represented tradeoff relationships between paired ESF. Correlation coefficients with large absolute values indicated weak relationships.

Quantification of landscape pattern

To comprehensively characterize the landscape's spatial pattern, the selected indicators were used to synthetically reflect features, including landscape diversity, fragmentation degree, and spatial heterogeneity^{72–74}. The final determination of these indices was made using a blend of multivariate covariance tests (Appendix B): patch density (PD), landscape percentage (PLAND), mean patch size (AREA_MN), largest patch index (LPI), Shannon's diversity index (SHDI), edge density (ED), landscape shape index (LSI), and interspersion and juxtaposition index (IJI). These measurements are described in detail in FRAGSTAT v4.2.⁷⁵.

Interactions between landscape formation and the compromises and cooperative effects among ecosystem service functions, as identified via GTWR

The GTWR model incorporated the time dimension and temporal and spatial local variability. This allowed the effective processing of spatiotemporal non-stationarity and estimation of factor parameters to address shortcomings in the GWR model and improve parameter estimation accuracy^{74,76,77}. Hence, the GTWR model was employed to examine the changing influence of landscape pattern in the YREB on the ES connections from 1990 to 2020. The model calculation is represented by Eq. (1):

$$Y_i = \beta_0(x_i, y_i, t_i) + \sum_{k=1} \beta_k(x_i, y_i, t_i) X_{ik} + \varepsilon_i \quad (1)$$

where Y_i signifies the dependent variable for the i th instance, X_{ik} denotes the k th independent variable for the i th instance, and (x_p, y_p, t_p) represents the spatiotemporal coordinates of the i th instance; $\beta_0(x_p, y_p, t_p)$ represents the intercept value, $\beta_k(x_p, y_p, t_p)$ encompasses a collection of parameter values for the i th instance, and ε_i is the random error.

The local regression coefficient of GTWR is estimated based on locally weighted least squares and can be expressed as:

$$\hat{\beta}(u_i, v_i, t_i) = [X^T W(u_i, v_i, t_i) X]^{-1} X^T W(u_i, v_i, t_i) Y \quad (2)$$

where the weighting matrix $W(u_p, v_p, t_p)$ is an $m \times n$ diagonal matrix and $W((u_p, v_p, t_p)) = \text{diag}(W_{11}, W_{12}, \dots, W_{ij}, \dots, W_{nn})$. W_{ij} ($1 \leq j \leq n$) is the spatiotemporal distance decay function, which is determined by the spatiotemporal distance and bandwidth⁷⁸.

In the GTWR model, each observation has a unique spatiotemporal weight matrix, and the degree to which the regression coefficient of an observation is influenced by other observations decays with increasing spatiotemporal distance. In this study, the Euclidean distance and Gaussian distance-decay-based functions are used to calculate the spatiotemporal weights⁷⁹. The mathematical expression is:

$$w_{ij} = \exp \left[-\left(d_{ij}^{ST} \right)^2 / h^2 \right] \quad (3)$$

$$d_{ij}^{ST} = \sqrt{\lambda [(u_i - u_j)^2 + (v_i - v_j)^2] + \mu (t_i - t_j)^2} \quad (4)$$

where d^{ST} is the spatiotemporal distance; λ and μ are the spatial factor and distance factor, respectively; h is the bandwidth. The optimal bandwidth is chosen based on the minimum cross-validation (CV) value.

To validate the performance of the GTWR, the results were compared with those of the OLS and GWR models. To evaluate the statistical parameters, analysis of variance (ANOVA) was performed^{80–82}.

Results

Changes in ecosystem service functions and trade-offs and synergies from 1990 to 2020

Alterations in ecosystem functions

Despite the spatial differences in environmental distribution across the YREB, their spatial configurations largely remained consistent (Fig. 3). In 2020, the total CS, FS, HQ, WR, and SC in the YREB were 24,921.10 million tons, 23.91 million tons, 0.75, 27,062, 248.08 billion m³, and 112,119.37 million tons, respectively. From 1990 to 2020, the combined total for FS, WR, and SC increased slightly, with only WR demonstrating a consistent upward trend. Conversely, FS and SC exhibited varying degrees of decline from 1990 to 2000 before experiencing a rapid resurgence. Meanwhile, CS and HQ decreased significantly. The catchment-level CS, FS, HQ, WR, and SC ranged from 7.42 to 243.17 million tons, 0.11 to 3.07 million tons, 0.27 to 0.96, 1.60 to 110.97 billion m³, and 0.20 to 3818.50 million tons, respectively. The five environmental distribution models exhibited variations in their spatial distribution patterns. The CS values were notably scattered, with catchments possessing elevated HQ. The SC values predominantly clustered in the upper and middle sections of the Yangtze Rubber River, while basins with higher FS and WR values were primarily found in the middle and lower sections. Spatially, there was an increase in CS and the headquarter values in the western and central areas. However, the reduction was most pronounced in the eastern region. The areas where WR and SC values increased were focused primarily in the central region, whereas the southwestern region exhibited a more noticeable decrease. Additionally, changes in FS values were relatively complex.

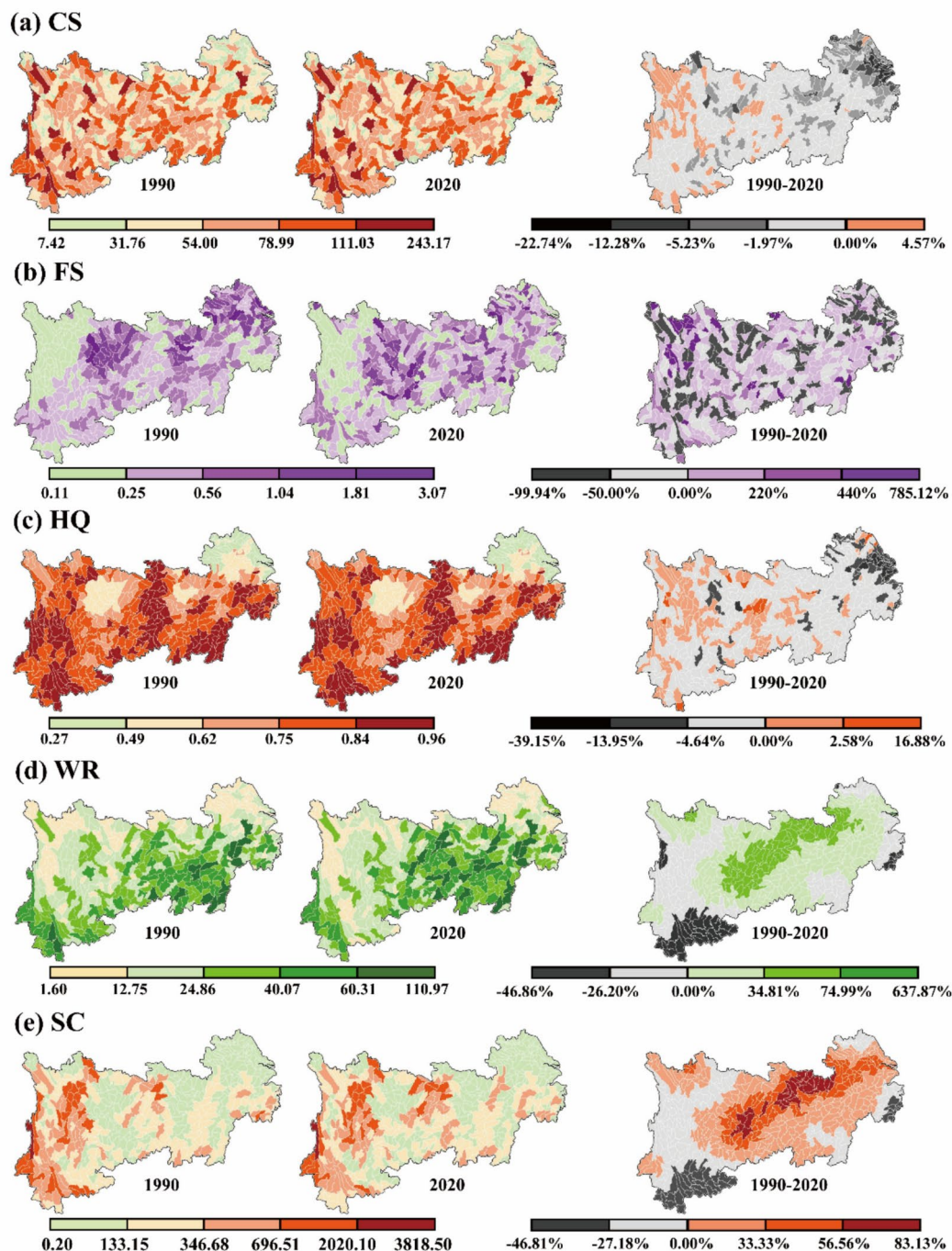


Fig. 3. Distribution and changes of CS (carbon sequestration), FS (food supply), HQ (habitat quality), WR (water retention), and SC (soil conservation) in the YREB. The measurements for CS, FS, HQ, WR, and SC are respectively in million tons, million tons, none, million cubic meters, and million tons. Maps were drawn by authors, using ArcGIS 10.8 (Environmental Systems Research Institute, USA. <https://www.esri.com/>).

Based on the SDE and COGM analyses (Fig. 4), the center point of the CS exhibited minor variations, primarily moving west from Laifeng County, situated in the central portion of the Yangtze River, toward Youyang County, in the river's upper sections. Overall, the FS centroid primarily moved toward the west, although a minor setback occurred in 2010. This was consistently observed within Longshan County, in the central part of the Yangtze River, throughout the time period. The centroid of the HQ predominantly shifted westward, remaining within Longshan and Youyang Counties in the upper reaches of the mountaintop Yangtze River across the four periods. The centroids of WR and SC exhibited substantial fluctuations, following a "west–east–west" migration pattern. The area of the standard deviation ellipse for CS increased, indicating spatial expansion and reduced concentration. The areas of the standard deviational ellipses for the other ESF contracted to varying degrees.

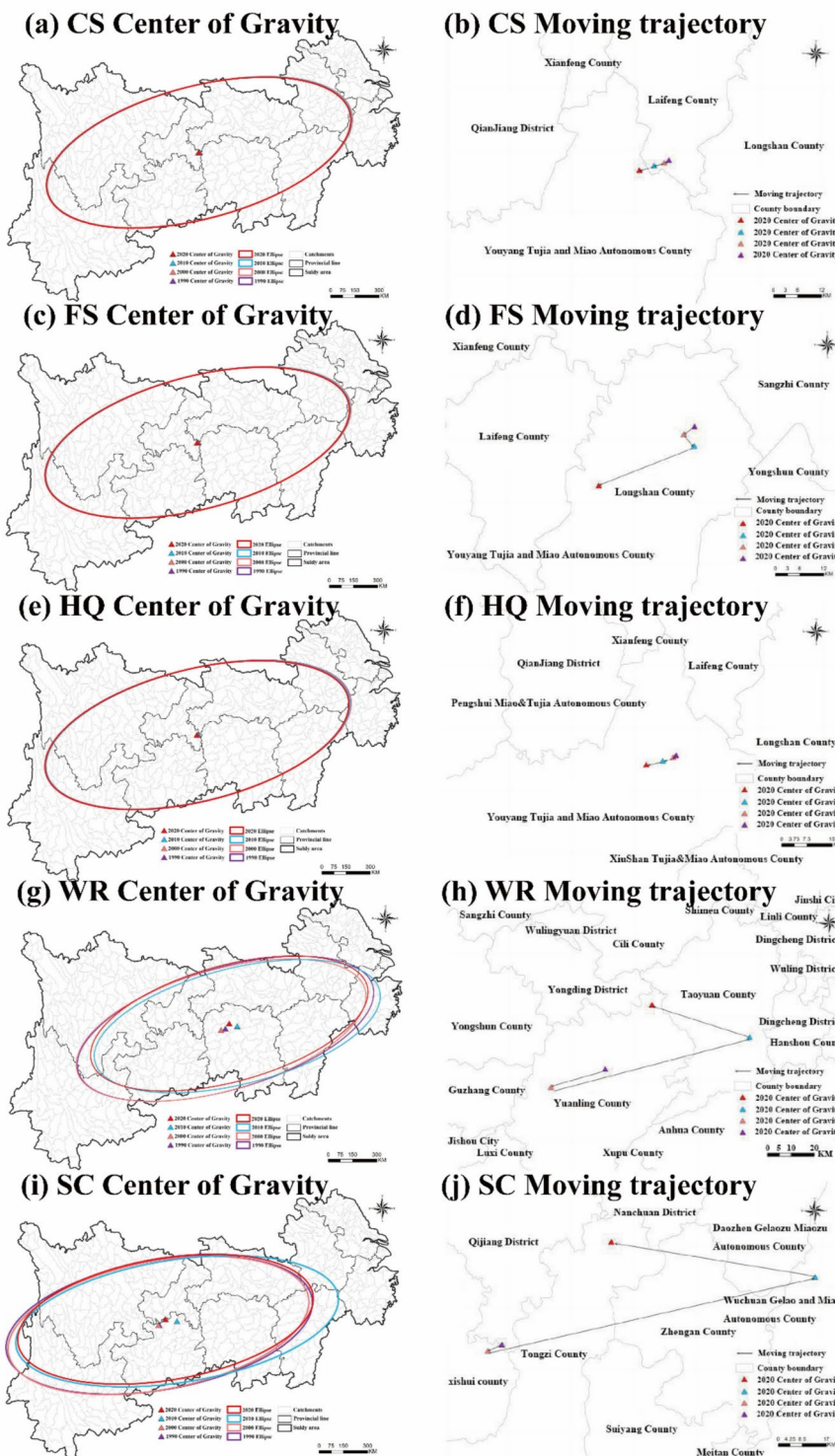


Fig. 4. Elliptic distribution of ES standard deviations and changes in center of gravity migration trajectory in 1990, 2000, 2010, and 2020. Maps were drawn by authors, using ArcGIS 10.8 (Environmental Systems Research Institute, USA. <https://www.esri.com/>).

Alterations in the balance and mutual benefits of ecosystem service functions

Overall, ESF exhibited a trend of transitioning from trade-off to synergy, with particularly pronounced changes observed in CS-FS, FS-HQ, FS-WR, and FS-SC. the transformation in CS-FS was the most drastic shift from weak trade-offs (-0.29) to synergistic (0.20). Although CS-WR, HQ-WR, and WR-SC were all in a state of synergy, the intensity declined to varying degrees, with strong significant correlations between CS, HQ, and

the other ecosystems ($p < 0.01$). FS-WR exhibited strong significant relationships only in 2010 ($p < 0.01$), characterized by trade-offs. FS-SC showed significant relationships only in 2010 ($p < 0.05$), indicating synergy. By 2020, all ESF exhibited synergy, with FS-WR showing weak synergy and FS-SC exhibiting moderate synergy. Other ESF demonstrated high levels of synergy, particularly CS-HQ, with a correlation coefficient > 0.93 (Fig. 5).

At the spatial scale, distinct ESF exhibited notable spatial disparities in their trade-offs and synergies (Fig. 6). Regarding CS, HQ and SC considerably influenced the ESF; however, their impact on FS was relatively minor (Fig. 6a–d). During 1990 to 2020, the correlation coefficient between CS and HQ increased slightly, with areas of high synergy primarily found in the central–western region, while trade-off areas were largely concentrated in the northeast corner. The powerful compromise zones between the CS and FS slowly diminished and were primarily located in the northern region of the YREB. Strong synergy areas exhibited an increasing-to-decreasing trend, primarily in the central area. The synergy between CS and SC showed a gradually decreasing trend, with strong synergy primarily distributed northeast of the YREB and fewer weak tradeoff areas distributed in the southwest corner. A pattern of growing collaboration was detected between the CS and WR, later succeeded by a pattern of diminishing collaboration. The strong collaboration was predominantly observed in the central–eastern area, while the compromises were located predominantly in the western region.

The relationships between FS and other ESF were more intricate (Fig. 6e–g). During 1990–2020, the FS-HQ synergy showed a gradual upward trend, which was not significant from 1990 to 2010; however, synergistic areas increased from 2010 to 2020 and were largely in the eastern and central regions, while trade-off areas were primarily in the western regions. FS-WR and FS-SC exhibited downward trends. The synergy and trade-off of FS-WR were primarily concentrated in the central and northwest/southwest aspects of the study zone, respectively, while those of FS-SC were mainly located in the northwest region.

From the perspectives of HQ and WR, during 1990–2020, HQ exhibited a stronger negative impact on SC in 2020, with most synergy areas converting into trade-off areas (Fig. 6h). HQ-WR maintained a relatively stable trade-off synergy relationship. Moreover, strong synergy between WR and SC was primarily observed in the northeastern area.

Spatiotemporal dynamics of landscape pattern characteristics from 1990 to 2020

Between 1990 and 2020, the landscape pattern of the YREB underwent significant changes due to alterations in land use, exhibiting increased landscape heterogeneity, diversity, fragmentation, and intricacy of patch shapes (Fig. 7). At the landscape level, elevations in the SHDI, ED, and LSI indicated an increased level of fragmentation and complexity. The decrease in LPI suggested an enlargement of non-dominant patches, whereas IJI remained relatively stable. At the class level, reductions in PLAND and AREA_MN, coupled with an increase in PD, indicated a decrease in agricultural land area and an increase in fragmentation.

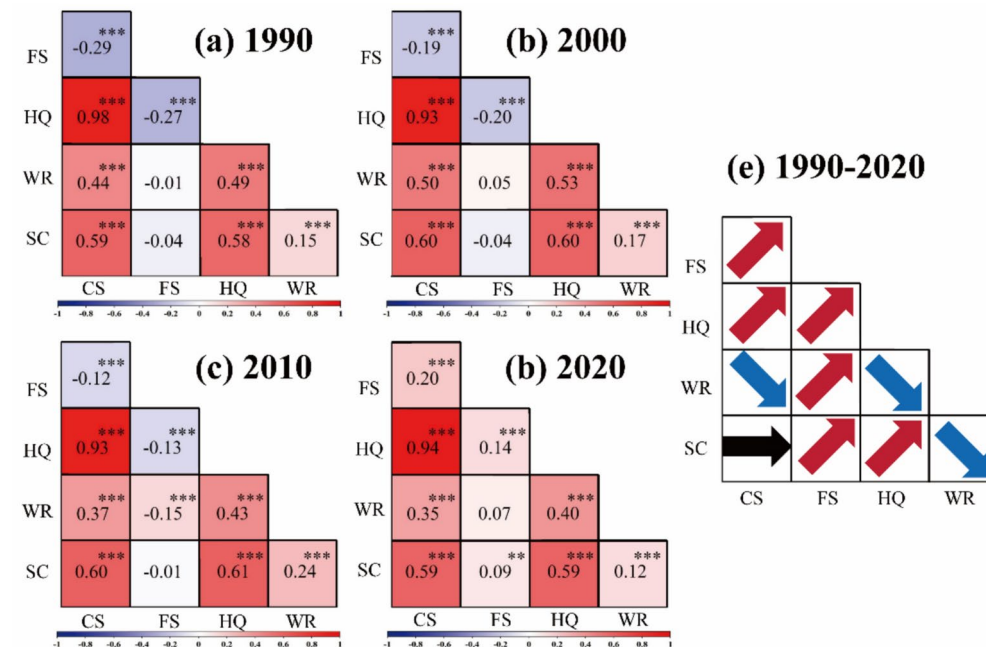


Fig. 5. Correlations among ES pairs ($*p < 0.05$; $**p < 0.01$; $***p < 0.001$) in 1990, 2000, 2010, and 2020 and correlation changes (red arrows: relationships were optimized in a synergistic direction, red arrows: relationships deteriorated in a trade-off direction, red arrows: relationships stayed the same).

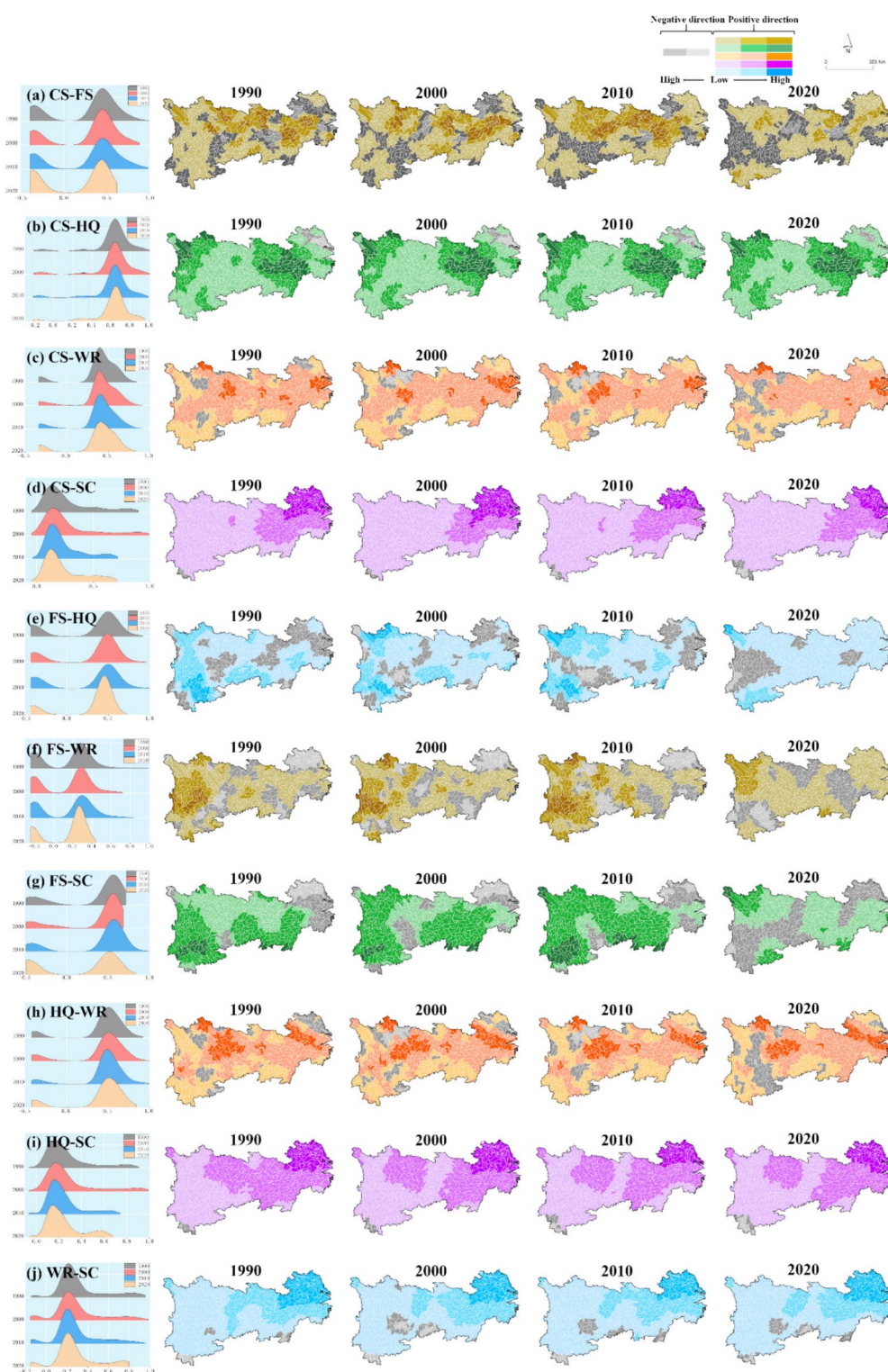


Fig. 6. Elliptic distribution of ES standard deviation and changes in center of gravity migration trajectory in 1990, 2000, 2010, and 2020. Maps were drawn by authors, using ArcGIS 10.8 (Environmental Systems Research Institute, USA. <https://www.esri.com/>).

GTWR analysis of the relationship between landscape pattern and ecological service systems Determining connections through the GTWR model

To identify suitable explanatory variables for constructing each service prediction model, the link between landscape factors and ES and their multicollinearity were evaluated. Regression analysis was employed to conduct multicollinearity tests on all variables after logarithmic transformation. Excluded from consideration

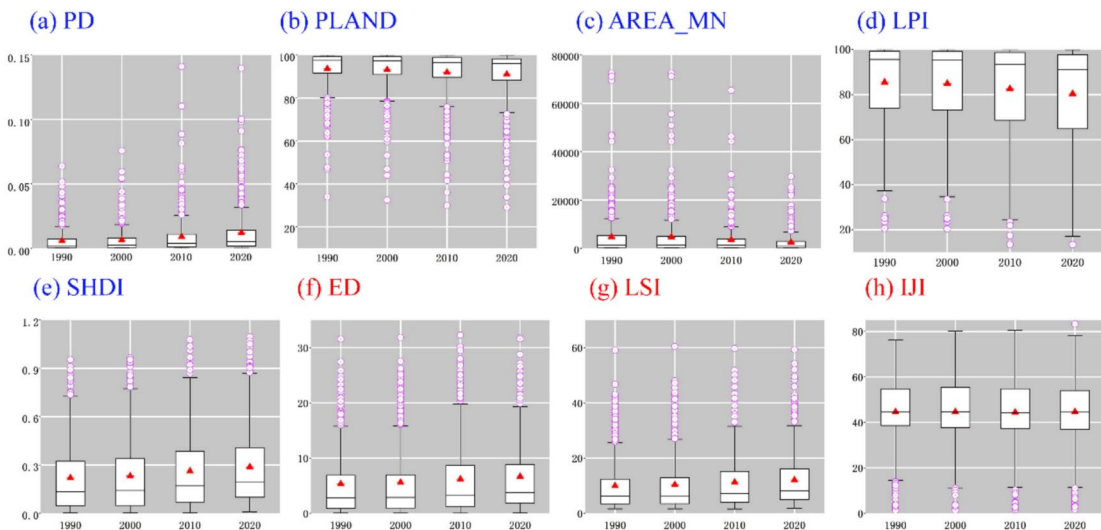


Fig. 7. Variation in landscape metrics regarding composition (a–e) and configuration (f–h).

were variables with variance inflation factors (VIF) greater than 10. The analytics-regression linear-collinearity diagnostic tool in SPSS26.0 was used for operation, in which PD, PLAND, AREA_MN, LPI, SHDI, ED, LSI, IJI and AI were selected as independent variables, and 10 groups of TS-ESF were respectively selected as dependent variables for collinearity diagnosis. Finally, among the selected 9 landscape variables, 8 variables show statistically significant correlations with ESF, and there is no severe multicollinearity among them. GTWR outperformed OLS and GWR based on the R^2 values of all indicators (Table 3). In the instance of GTWR, the R^2 estimation for FS-SC increased to 0.455 and 0.151 more than OLS and GWR, respectively. Moreover, the RSS and AICc values of the Akaike information criterion and the residual sum of squares were represented by the model, respectively. The smaller the values of both indicators, the closer the fit between the model and observed data. The RSS of the GTWR model was 95.681 and 31.842 lower than that of the OLS and GWR models, respectively, suggesting a notable increase in the accuracy of the GTWR prediction. Furthermore, among all ESF, excluding CS-HQ, CS-WR, and HQ-WR, GTWR had the lowest AICc, implying that the GTWR model was most appropriate for modeling the connection between ESF and landscape pattern. On the whole, the GTWR model exhibits the lowest AICc value and the highest R-squared value, with no significant spatio-temporal autocorrelation in the residuals. This suggests that the GTWR model possesses the strongest explanatory power for spatio-temporal heterogeneity while effectively controlling overfitting. Consequently, the GTWR model quantifies proximity via a spatiotemporal joint weighting function, thereby addressing the limitation of separating spatio-temporal dimensions inherent in traditional models. This highlights the theoretical distinctiveness and practical superiority of the GTWR model in modeling spatio-temporal non-stationarity. Therefore, this study selects the GTWR model for analysis.

The GTWR showed high accuracy in predicting ESF. Based on most ES metric prediction models, the selected landscape pattern variables had a high degree of interpretation for ESF, excluding CS-FS, FS-HQ, and HQ-WR. Most prominently, the accuracies reached 91.83%, 91.18%, and 91.05% for CS-SC, HQ-SC, and WR-SC, respectively. The ESF were impacted by landscape variables in positive and negative ways. Moreover, the ESF responded differently to landscape variables, occasionally exhibiting opposite directions. Regarding the impact of landscape variable indices on CS-HQ, LSI exhibited positive correlations across all catchments, whereas ED exhibited negative effects. In addition, landscape composition made a greater contribution to ESF, as indicated by the regression coefficients having larger absolute values than the configuration metrics (Table 4).

Within the comprehensive regression outcomes, excluding CS-FS and CS-HQ, all selected landscape variables exhibited significant effects on the ESF at different levels. Additionally, all variables demonstrated strong significant relationships with HQ-SC and WR-SC ($p < 0.01$). Among the impact relationships of different landscape variables with ESF, besides maintaining consistent impacts on CS-SC, HQ-SC, and WR-SC, the landscape variables exhibited varied directions of influence on the other ESF. The predictive models for CS-SC, HQ-SC, WR-SC, PD, ED, LSI, and SHDI positively affected the ESF, whereas the other variables exhibited negative effects. The order of the absolute magnitude of influence was ED > SHDI > LSI > PLAND > LPI > PD > AREA_MN > IJI.

Spatiotemporal relationship patterns

The extent to which different variables in the YREB impact ESF in different basins varied significantly, necessitating consideration of the spatiotemporal heterogeneity of landscape variables at a local scale. To investigate their associations' heterogeneity and spatiotemporal correlation, the annual average regression coefficients of the landscape variables for each basin were summarized and visually processed for each basin. The average regression coefficients of landscape variables for different basins in different periods are shown in Fig. 7; the spatiotemporal patterns of landscape variables' relationships and ESF are displayed in Figs. 10, 11, 12, 13

Variable	Model	R ²	RSS	AICc
CS-FS	OLS	0.071	144.779	521.550
	GWR	0.302	108.832	98.117
	GTWR	0.426	90.206	-50.239
CS-HQ	OLS	0.302	132.409	352.208
	GWR	0.694	58.071	-1092.820
	GTWR	0.701	57.632	-998.753
CS-SC	OLS	0.711	264.346	1663.035
	GWR	0.906	86.057	-347.052
	GTWR	0.918	74.808	-420.396
CS-WR	OLS	0.131	278.324	1760.729
	GWR	0.475	168.077	922.147
	GTWR	0.506	162.861	970.848
FS-HQ	OLS	0.054	651.226	3372.463
	GWR	0.267	504.618	3006.570
	GTWR	0.447	380.894	2665.530
FS-WR	OLS	0.103	913.482	4014.084
	GWR	0.390	621.456	3401.440
	GTWR	0.529	480.041	3156.450
FS-SC	OLS	0.306	146.007	537.565
	GWR	0.610	82.168	-434.746
	GTWR	0.761	50.326	-1119.700
HQ-WR	OLS	0.057	299.803	1901.679
	GWR	0.416	185.751	1111.720
	GTWR	0.447	175.815	1138.870
HQ-SC	OLS	0.706	262.120	1647.002
	GWR	0.900	89.002	-283.267
	GTWR	0.9118	78.590	-326.892
WR-SC	OLS	0.714	201.010	1143.712
	GWR	0.903	68.035	-792.584
	GTWR	0.9105	62.852	-811.452

Table 3. ANOVA between the GTWR and OLS/GWR model.

Y\X	CS-FS	CS-HQ	CS-SC	CS-WR	FS-HQ	FS-WR	FS-SC	HQ-WR	HQ-SC	WR-SC
PD	0.073*** (0.001)	-0.170*** (0.000)	0.469*** (0.000)	0.272*** (0.000)	-0.122*** (0.000)	-0.143*** (0.000)	-0.212*** (0.000)	0.119*** (0.000)	0.435*** (0.000)	0.442*** (0.000)
PLAND	-0.04 (0.079)	0.320*** (0.000)	-0.673*** (0.000)	0.286*** (0.000)	0.169*** (0.000)	0.170*** (0.000)	0.353*** (0.000)	-0.112*** (0.000)	-0.651*** (0.000)	-0.673*** (0.000)
AREA_MN	-0.101*** (0.000)	0.016 (0.491)	-0.301*** (0.000)	-0.172*** (0.000)	0.124*** (0.000)	0.128*** (0.000)	0.131*** (0.000)	-0.130*** (0.000)	-0.294*** (0.000)	-0.257*** (0.000)
LPI	-0.115*** (0.000)	0.210*** (0.000)	-0.504*** (0.000)	0.297*** (0.000)	0.142*** (0.000)	0.141*** (0.000)	0.277*** (0.000)	-0.174*** (0.000)	-0.483*** (0.000)	-0.468*** (0.000)
SHDI	0.072*** (0.002)	-0.251*** (0.000)	0.720*** (0.000)	0.309*** (0.000)	-0.182*** (0.000)	-0.184*** (0.000)	-0.373*** (0.000)	0.139*** (0.000)	0.694*** (0.000)	0.715*** (0.000)
ED	0.019 (0.407)	-0.351*** (0.000)	0.804*** (0.000)	0.292*** (0.000)	-0.219*** (0.000)	-0.255*** (0.000)	-0.482*** (0.000)	0.141*** (0.000)	0.792*** (0.000)	0.636*** (0.000)
LSI	0.025 (0.275)	0.239*** (0.000)	0.702*** (0.000)	0.304*** (0.000)	-0.187*** (0.000)	-0.221*** (0.000)	-0.392*** (0.000)	0.159*** (0.000)	0.684*** (0.000)	0.683*** (0.000)
IJI	0.156*** (0.000)	0.031 (0.174)	-0.050** (0.031)	0.054** (0.018)	0.052** (0.022)	-0.089*** (0.000)	0.064*** (0.006)	0.049** (0.034)	-0.078*** (0.001)	-0.101*** (0.000)

Table 4. Outcomes of spatial regression analysis on the landscape pattern and TS-ESF in the YREB. *p<0.05; **p<0.01; ***p<0.001. In parentheses are the p-values of the coefficients.

and 14 and Fig. S1–S5, respectively. Herein, only the distributions of the five simulated models, namely CS-HQ, CS-SC, FS-SC, HQ-SC, and WR-SC, are presented; the remaining distributions are available in Appendix C.

The influence of landscape variables on TS-ESF was not constant, with certain variables changing in magnitude and direction over time (Figs. 8, 9). For example, in the CS-FS relationship, ED exhibited predominantly negative impacts across watersheds from 1990 to 2010. However, by 2020, the proportion of watersheds with positive



Fig. 8. Wind direction chart for mean regression coefficient of CS-FS, CS-HQ, CS-SC, CS-WR, and FS-HQ.

impacts increased to 74.37%, highlighting a more pronounced positive correlation. The positive relationship with LPI diminished over time, with all watersheds exhibiting negative impacts by 2020, whereas the magnitude of LSI's negative impacts decreased annually. Additionally, the dominant AREA_MN relationship underwent a transition from positive to negative and was ultimately restored to positive (Fig. 8a). In the CS-SC relationship, the negative AREA_MN relationship exhibited an "increase-decrease-increase" transition. For the FS_SC relationship, the SHDI shifted from entirely positive impacts to 52.73% of watersheds exhibiting negative impacts by 2020, with the average regression coefficient slightly higher than that of the positive impacts. ED transitioned from entirely negative impacts to 21.43% of the watersheds exhibiting positive impacts by 2020, with the average regression coefficient slightly exceeding the negative impacts (Fig. 8c). Certain landscape variables maintained a consistent relationship with ESF over many years. For example, ED and AREA_MN consistently maintained positive and negative impacts across all watersheds in CS_SC and HQ_SC, respectively (Figs. 8c, 9c).



Fig. 9. Wind direction chart for mean regression coefficient of FS-SC, FS-WR, HQ-SC, HQ-WR, and WR-SC.

Among the five models with a higher model fit, CS-HQ, PLAND, LPI, LSI, AREA_MN, and IJI positively affected CS-HQ; however, only PLAND and LPI exhibited significant relationships ($p < 0.01$). Although most basins positively impacted the PD, their effect on CS-HQ was negative. From 1990 to 2020, the region with a high concentration of positive coefficients shifted in the YRB's upper and lower reaches. The regions with high concentrations of positive coefficients for PLAND and SHDI were most abundant in the middle of the YRB, whereas LPI was primarily distributed downstream of the YRB. The primary habitats of areas with high concentrations of negative coefficients for ED were in the middle and lower portions of the Yangtze River. Meanwhile, IJI, which showed a higher concentration of negative impact areas, was mainly distributed upstream of the Yangtze River Delta (Fig. 10). An equal number of positive and negative landscape variables were present in the CS-SC relationship. Among them, the ED coefficient was the highest at 0.804 and significant at the 1%

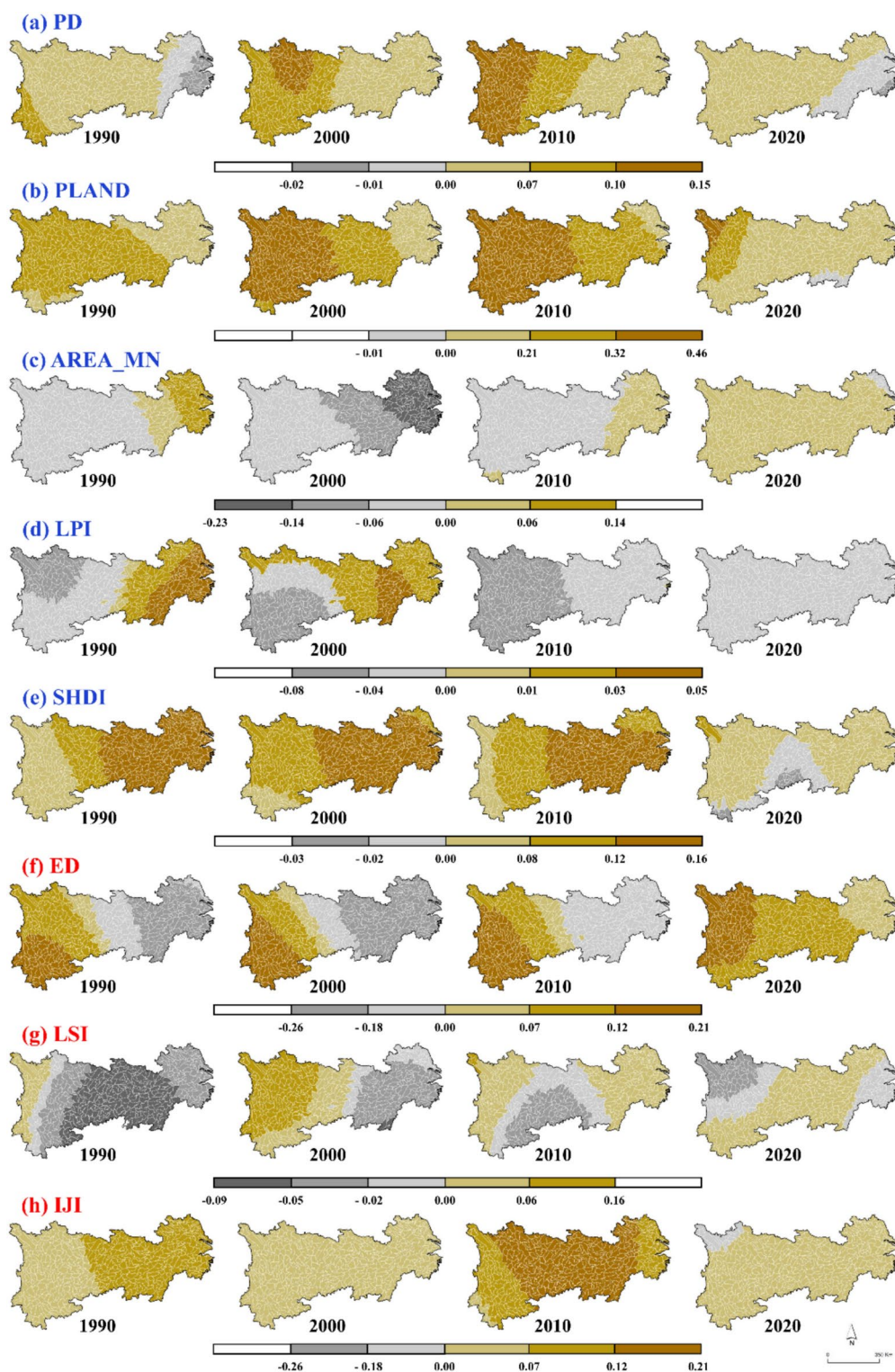


Fig. 10. Spatial patterns of regression coefficients in estimating CS–HQ in 1990, 2000, 2010, and 2020. Maps were drawn by authors, using ArcGIS 10.8 (Environmental Systems Research Institute, USA. <https://www.esri.com/>).

level, exhibiting a "high-low-high" distribution of regression coefficients from upstream to downstream. PD, PLAND, LSI, and AREA_MN, predominantly influenced by negative effects, exhibited varying degrees of downstream-high and upstream-low distribution characteristics. Conversely, the LPI and SHDI exhibited a distribution in which the upstream areas were negative and the downstream areas were positive. In contrast, the IJI showed spatial differentiation, with positive trends in upstream areas and negative trends in downstream

areas. Moreover, high-value positive coefficient areas radiated outward from the northwestern part of Sichuan Province and gradually contracted over time (Fig. 11). Regarding the FS–SC relationship, the absolute values of the ED regression coefficient and LSI were relatively high; all landscape variables were significant at the 1% level. Significant distributions of each landscape variable were found in spatial differences, leading to varying changes over time. For example, the high-value area of the positive coefficients for PLAND shifted from upstream to downstream.

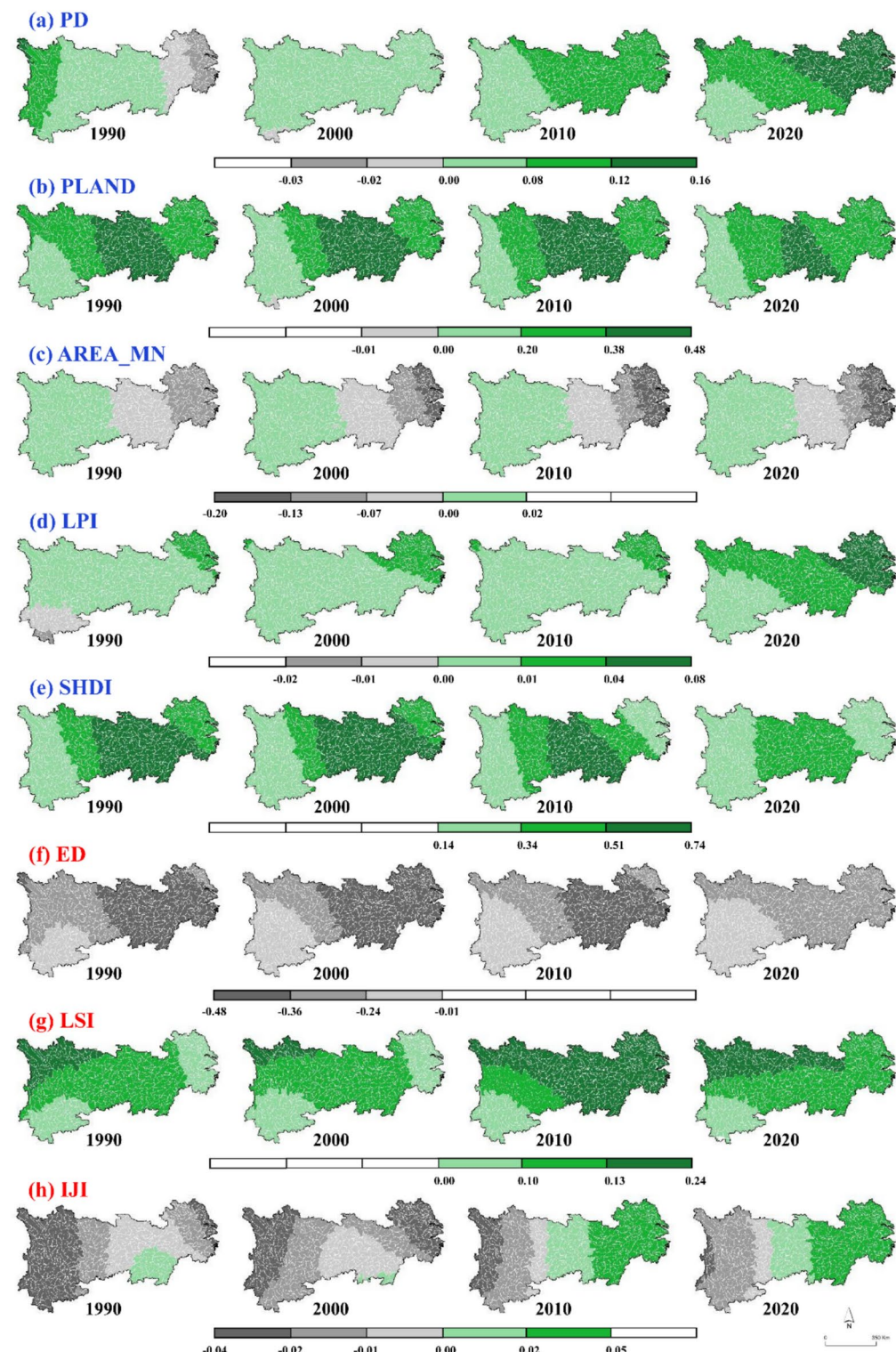


Fig. 11. Spatial patterns of regression coefficients in estimating CS–SC in 1990, 2000, 2010, and 2020. Maps were drawn by authors, using ArcGIS 10.8 (Environmental Systems Research Institute, USA. <https://www.esri.com/>).

midstream areas with varying degrees of coefficient reduction, transforming into negative impacts downstream. A high-value area of negative coefficients for ED was primarily distributed in the midstream areas, with coefficient values showing varying degrees of decline over time (Fig. 12). The regression coefficients of HQ-SC and WR-SC exhibited certain similarities, with the direction and ranking of landscape variable effects largely consistent; however, there were certain spatial variations. In the HQ-SC relationship, apart from PD and IJI, the

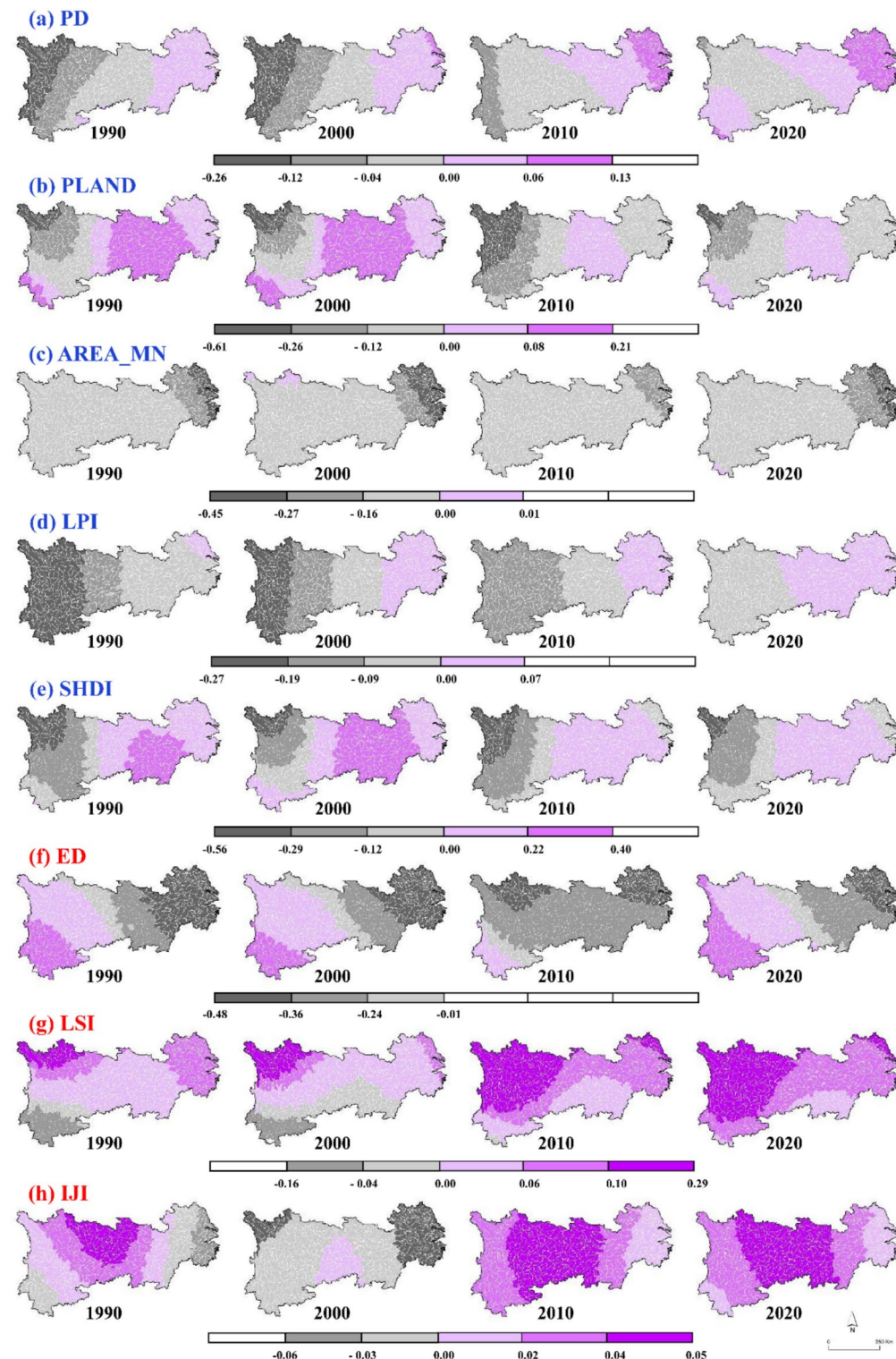


Fig. 12. Spatial patterns of regression coefficients in estimating FS-SC in 1990, 2000, 2010, and 2020. Maps were drawn by authors, using ArcGIS 10.8 (Environmental Systems Research Institute, USA. <https://www.esri.com/>).

spatiotemporal distribution changes of the other landscape variables were relatively small. Specifically, negative coefficient values for PD were distributed along the YRB from northwest to southeast in 1990 and gradually decreased. By 2020, the distribution of coefficient values along the YRB was positive, negative, and positive, respectively. In addition, IJI primarily had a positive impact, with its high-value area mainly concentrated on the Yangtze River's middle reaches. Moreover, IJI underwent a transition from positive to negative impact in the upper and lower reaches of the Yangtze River in 2000 (Fig. 13). In the WR-SC relationship, apart from PLAND and AREA_MN, the spatiotemporal distribution changes of the other landscape variables were relatively minor. Specifically, PLAND was primarily characterized by a negative impact, and the high-value area of the negative impact shifted from the upper reaches to the middle-upper reaches. The coefficient values of AREA_MN transitioned from "positive-negative-positive" from west to east in 1990 to "positive-negative" in 2020 (Fig. 14).

Among the five models with a low model fit, the degree of fitting was the lowest in CS-FS ($R^2=0.426$), and the associated relationship was primarily characterized by a positive influence, with IJI having the greatest impact. In addition, there was no significant relationship between PLAND, ED, LSI, and CS-FS. The upper reaches of the northern Yangtze River basin were the focal point for the high-value positive coefficients of PD, PLAND, ED, and LSI in relation to their spatial distribution, whereas AREA_MN, IJI, and SHDI were primarily concentrated in the downstream region. Furthermore, the coefficient values of LPI transitioned from "positive-negative" from west to east in 1990 to an entirely negative impact distribution (Fig. S1). Excluding AREA_MN, all landscape variables positively correlated with CS-WR, with SHDI having the highest impact. Due to the complex relationship between the CS and WR, significant differences existed in their spatial distributions. Typically, PD and LPI displayed a positive distribution in the upstream area and a negative distribution in the downstream area. The coefficient values of ED showed a "positive-negative" distribution from west to east, with the proportion of negatively affected basin areas reaching 94.54% in 2010 (Fig. S2). In the FS-HQ relationship, LPI had the highest impact, with a value of 0.297. Apart from IJI, which had a significant correlation with FS-HQ at the 5% level, all other landscape factors were statistically significant at the 1% level. The coefficient values of PD and the upper reaches of the LSI showed a negative and southwest spatial distribution. In the mid-lower reaches region, a positive distribution was observed. The coefficient values of LPI, AREA_MN, IJI, and SHDI transitioned primarily from positive to negative (Fig. S3). In the FS-WR relationship, negative impacts were predominant, with ED exhibiting the most significant negative influence. Similar to the spatial distribution of CS-WR, there were significant differences; for example, the coefficient values of LPI were predominantly positively influenced in 1990, but by 2000, negative relationships increased in the upstream region of the Yangtze River. By 2010, negative relationships dominated, and in 2020, a shift toward an "eastward" distribution of positive-negative influences occurred. The coefficient values of the SHDI shifted from entirely positive influences in 1990 to partially negative influences in the downstream areas by 2020 (Fig. S4). Positive impacts were predominant in the HQ-WR relationship, with LSI exhibiting the greatest positive influence. The spatiotemporal distributions of the coefficient values for LPI, ED, AREA_MN, and SHDI remained relatively stable. High-value areas with negative coefficients for PLAND were concentrated in the upstream regions of the Yangtze River, positive coefficients were concentrated in downstream regions, and low-value areas were concentrated upstream, with coefficient values decreasing from 1990 to 2020 (Fig. S5).

Discussion

Mechanisms for landscape pattern constraining the relationship between ESF

The transformation of regional land use is directly mirrored in landscape patterns, and the acceleration of urbanization intensifies these fluctuations, leading to more noticeable landscape diversity. Building on our research findings, analyzing landscape patterns and ESF in more detail furthers our understanding of how landscape patterns influence ESF, offering new avenues for improving ESF by optimizing landscape patterns^{83,84}. To comprehensively elucidate their relationship, the GTWR model was adopted in the current study to predict the influence of five ESF on the values of watershed subsets concerning all landscape variables. SHDI, ED and LSI had significant effects on all ESF, while PD had significant effects only on CS and SC. Higher values of PLAND and AREA_MN for agricultural land corresponded to greater promotion of CS and FS, whereas an increase in PD led to CS and FS inhibition (Table 5 and Fig. 15). Additionally, the impact of other landscape indices on ESF was multifaceted, exhibiting positive and negative impacts consistent with the conclusions drawn by other researchers in this region^{85,86}. Over the past 30 years, the swift urban growth in the Yangtze Economic Belt has resulted in ecological space reduction and landscape division, among other issues, which have notably diminished the ability of urban ecosystems to store carbon. The fundamental cause of the decrease in regional carbon storage is the conversion of agricultural land to construction land^{85,87}. Although there was a noticeable reduction in the farmland area and a short-term drop in agricultural yield between 1990 and 2000, the rise in financial backing for farming, progress in agricultural techniques, and the introduction of strategies, including the development of high-quality fundamental farmland, establishing a permanent basic farmland protection boundary, and suggesting the "Development Plan Outline for the Yangtze Economic Belt," have contributed to a growing pattern in cereal production in the YREB from 2000 to 2020. By 2020, regional grain production increased by 24.85 million tons compared to 1990, effectively ensuring regional food production security⁸⁸. Furthermore, SC capacity demonstrated only a transient decline during 1990–2000, with sustained growth observed in subsequent periods. Analyses reveal that intensive development initiatives during the 1990s triggered ecological function deterioration and accelerated soil erosion. To counteract these impacts, China's 2020 Proposal by the CPC Central Committee on the Formulation of the 14th Five-Year Plan for National Economic and Social Development mandated strategic reorientation of the YREB from exploitation-dominated to conservation-oriented paradigms. This policy trajectory intensified post-2012 following the 18th National Congress of the Communist Party of China, reaching a milestone in 2014 with the Ministry of Ecology and Environment's issuance of Technical Guidelines for National Ecological Protection Red Line Delineation (Trial).

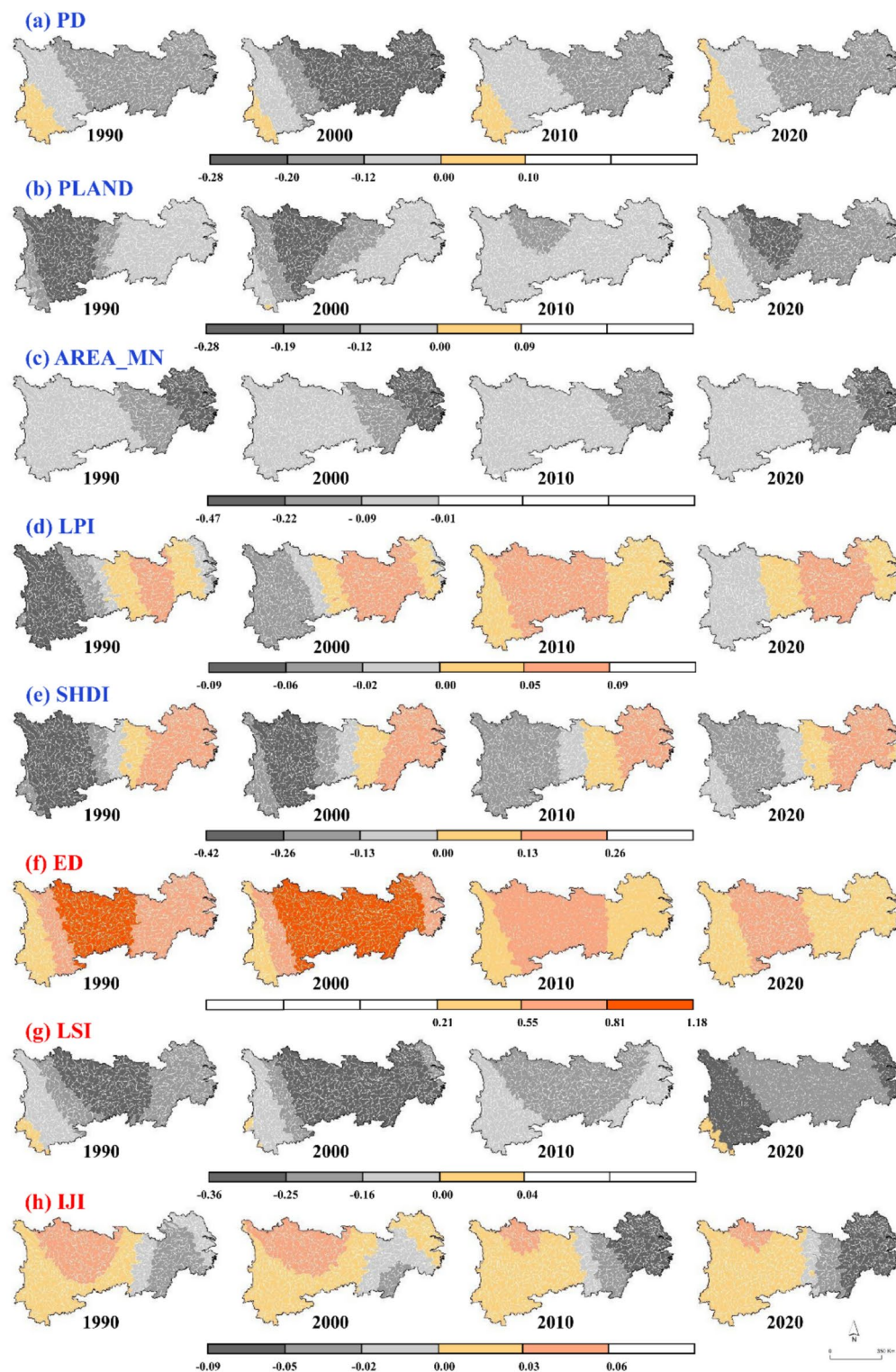


Fig. 13. Spatial patterns of regression coefficients in estimating HQ-SC in 1990, 2000, 2010, and 2020. Maps were drawn by authors, using ArcGIS 10.8 (Environmental Systems Research Institute, USA. <https://www.esri.com/>).

These guidelines initiated pilot ecological red line demarcations in Jiangxi and Hubei provinces, establishing a systematic conservation framework. Concerted implementation of the "One River, Two Corridors, Three Zones, Multiple Sources" restoration strategy has driven a 1.697 billion tons SC capacity increase during 2010–2020.

The characteristics exhibited by individual ESF were mostly consistent; the influence of landscape patterns among ESF was multifaceted, with the relationships even more complex than those of single ESF (Tables 4 and

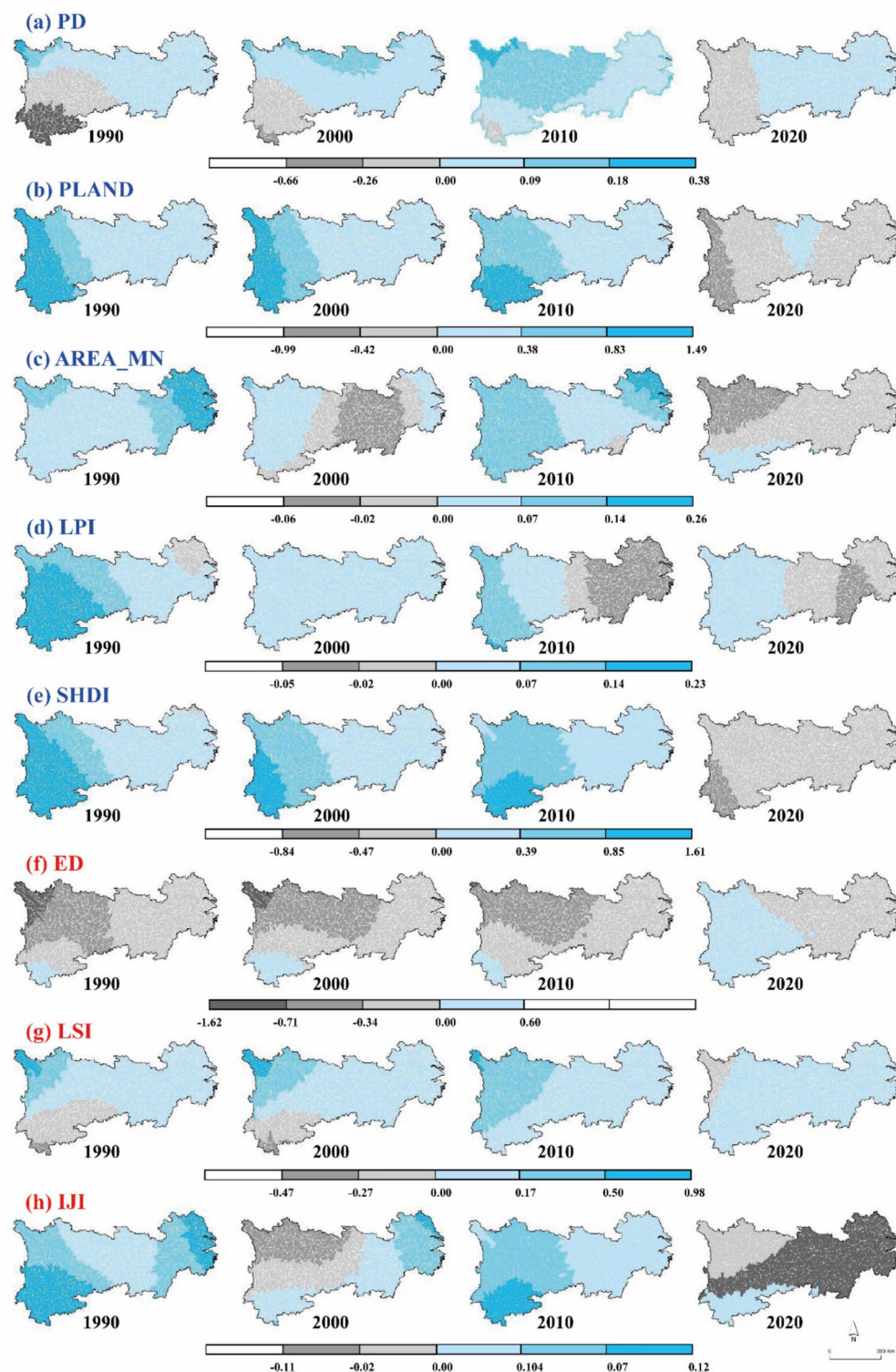


Fig. 14. Spatial patterns of regression coefficients in estimating WR-SC in 1990, 2000, 2010, and 2020. Maps were drawn by authors, using ArcGIS 10.8 (Environmental Systems Research Institute, USA. <https://www.esri.com/>).

5). First, changes in ESF were influenced by landscape patterns, which promoted or inhibited such changes. Specifically, the influence of landscape composition was beyond landscape arrangement; this aligns with findings from other regions, indicating that landscape composition is the primary factor influencing ES changes. These insights can assist decision-makers in selecting relatively reasonable spatial reconstruction choices among

Y\X	CS	FS	HQ	WR	SC
PD	-0.969** (0.026)	-0.044 (0.352)	0.459** (0.028)	0.248* (0.079)	0.147** (0.018)
PLAND	0.909** (0.035)	0.002 (0.213)	0.517 (0.138)	-0.121 (0.354)	-0.109** (0.026)
AREA_MN	0.238** (0.021)	0.132** (0.025)	0.196** (0.019)	-0.016 (0.352)	0.185** (0.027)
LPI	0.857** (0.019)	0.063** (0.020)	0.216** (0.018)	-0.003 (0.135)	-0.048* (0.063)
SHDI	0.264** (0.028)	0.199** (0.021)	-0.505** (0.023)	-0.178** (0.017)	-0.288** (0.015)
ED	0.171** (0.034)	0.268** (0.026)	-0.697** (0.029)	-0.236** (0.031)	-0.312** (0.024)
LSI	0.244** (0.031)	0.347** (0.024)	-0.629** (0.028)	-0.119** (0.030)	-0.282** (0.023)
IJI	0.730** (0.016)	0.080** (0.019)	-0.032 (0.265)	-0.004 (0.347)	-0.143** (0.018)

Table 5. Spatial regression analysis of landscape pattern and ESF in the YREB. * $p < 0.05$; ** $p < 0.01$; *** $p < 0.001$. In parentheses are the p-values of the coefficients.

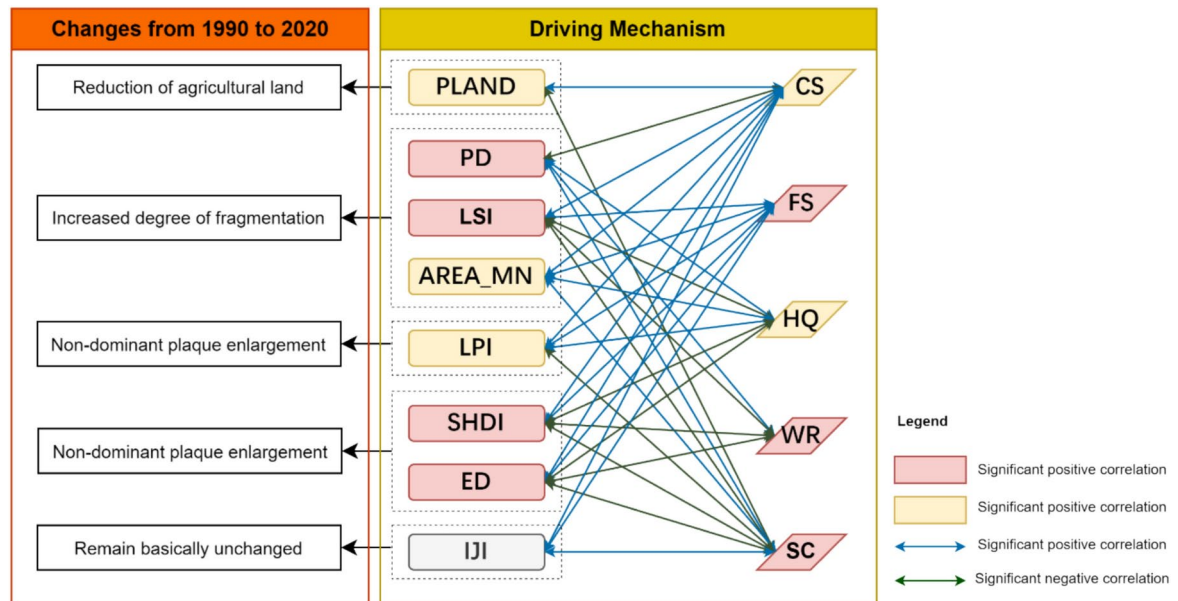


Fig. 15. Influential mechanisms of landscape patterns on ESF.

comparable strategic and optimized management of ESF in the YREB region by adjusting landscape types, patch densities, and other landscape patterns^{89,90}.

Second, GTWR can thoroughly explore the local spatiotemporal characteristics of the region, as it was combined with the complexity of the internal influence relationships among ESF; this approach resulted in significant differences from previous studies. In addition, the CS and FS values were primarily influenced by agricultural land, whereas the WR value was influenced by rainfall. Changes in agricultural land area and rainfall in the YREB region exhibited high randomness, resulting in greater instability in the landscape's spatiotemporal pattern indices among the three ESF (CS–FS, CS–WR, FS–HQ, and HQ–WR). These findings signify an improvement over previous studies^{91,92}. Furthermore, the impact that landscape pattern has on SC and other ESF (CS–SC, HQ–SC, HQ–SC, and WR–SC) was consistent with the most prominent impact on CS–SC. This suggests that landscape patterns have a comparatively steady impact on CS, benefiting from the outstanding contributions of decision-makers to soil conservation in regional land parcels. The SC value in the YREB decreased temporarily during 1990–2000 due to ecological space shrinkage. However, with the proposal of ecological environmental protection policies in the region, especially the delineation of ecological redlines in the along-river areas that mitigate the impact of rapid urbanization on watershed ecological environments, the SC increased by 2419.02 million tons from 1990 to 2020.

Finally, the impact of landscape pattern on ESF is a complex trade-off relationship, implying that it promotes one ES and suppresses others, requiring decision-makers to arrange different trade-offs based on development needs⁴⁷. For example, a reduction in agricultural land PD will promote the growth of FS while inhibiting the level of HQ improvement. These trade-offs require decision-makers to clarify the development goals for each region, such as whether to increase food supply capacity to balance the human–food supply–demand relationship or decrease its food production capacity to enhance biodiversity.

In summary, systematic analysis of ESF synergy–tradeoff relationships enhances understanding of landscape pattern-driven ESF dynamics within synergistic frameworks. This approach enables nature-aligned ecological

decision-making while avoiding unintended consequences from conventional siloed studies, which risk exacerbating ESF tradeoffs, reducing provisioning capacity, and causing secondary ecological damage.

Implications for sustainable landscape management

In this study, GTWR was employed to examine the model's estimated parameters across various periods and local regions within the YREB. From a spatiotemporal multidimensional perspective, the constraint mechanism of landscape patterns on the relationship between ESF was investigated^{93,94}. This approach provides technical support to accurately analyze the factors influencing ES landscape patterns. The study findings can guide the evolution of spatial management and strategic planning for numerous ESF, providing a reference for improving the adaptability of land use and its contribution to sustainable regional landscape management. An unreasonable LULC alters the pattern and distribution of land landscape patches, affecting ESF in the region. Degradation of certain ESF will result from this alteration, and ecological effects will be reduced³⁸. Therefore, decision-makers in regional planning should prioritize the dual choices of conservation and development^{95,96}. This requires that managers methodically define land use control zones in the "National Land Spatial Plan," considering the varying land use conditions across regions. They must apply distinct and accurate regulation over diverse economic zones to guarantee synchronized high-standard growth and superior protection. Considering the potential negative consequences, landscape interactions, particularly the protection of multifunctional landscapes, should be fully considered to maximize comprehensive benefits⁹⁷.

Limitations

Analyses of influencing factors may yield varying results due to their different scales. In the current study, analysis was only conducted at the catchment scale, lacking data for more microscopic grids and macroscopic provincial scales. Our catchment-level analysis may obscure finer-scale dynamics (e.g., County unit). Hence, multi-scale comparison is a crucial future direction. Moreover, due to the introduction of landscape pattern driving factors of ES relationships based on individual ESF, few studies have reported similar results, limiting the ability to make direct comparisons and perform validation analyses, leading to uncertainty in the final evaluation. In future studies, the scientific validity of this method can be further confirmed through application in other regions, providing a basis for the landscape management of ESF in other regions. Furthermore, while acknowledging the significant influence of landscape patterns on ESF, it is imperative to investigate the impact of climatic variables, such as precipitation and temperature, on the dynamics of ESF.

Conclusions

The relationships among ESF have become a research focal point and are considered crucial for sustainable landscape management. In this study, the dynamic responses of the relationships between five typical ESF and variation in landscape pattern in the YREB were systematically investigated. The GTWR model accurately explained the influencing mechanisms underlying ES relationships. Most landscape patterns significantly affect the relationships among ESF; however, these impacts were diverse, often requiring decision-makers to continuously balance landscape management. The purpose of this study was to offer scientific justification for policymakers to develop informed strategies based on the complex response mechanisms of inter-ecosystem relationships with landscape pattern.

The spatiotemporal patterns of ES tradeoffs and synergies and the landscape structural factors influencing them were also evaluated within the YREB over the past 30 years. The alterations in five ESF were derived from an analysis of the overall changes. Initially, swift urban growth greatly affected farming and ecological areas, this has resulted in a persistent decline in regional CS, with the total CS decreasing from 25.23 billion tons to 24.92 billion tons. Concurrently, HQ deteriorated from 0.76 to 0.75, indicating moderate degradation of landscape diversity and environmental quality across the YREB. Furthermore, the heterogeneity of the landscape is increasing, along with the diversity, fragmentation, and complexity of patch shapes. During the study period, ESF exhibited a trend of transitioning from trade-off to synergy, the transformation in CS-FS was the most drastic shift from weak trade-offs (-0.29) to synergistic (0.20). This conclusion clearly indicates that, despite the degradation of the landscape ecosystem, the changing trend from tradeoffs to synergies among ESF under the effective control of managers confirmed the effectiveness of the relevant decisions made during this period. In particular, the profound transformation of the CS-FS relationship clearly demonstrates that, despite its impact on arable land in the 1990s, China's increased investment in agriculture, advancements in agricultural technology, and the implementation of strategic measures such as developing high-quality basic farmland, delineating permanent basic farmland protection boundaries, and proposing the Outline of YREB Development Plan, have collectively promoted the effective enhancement of regional grain production. Consequently, the CS-FS relationship has evolved from one characterized by weak trade-offs to a state of synergy.

In conclusion, the contribution of landscape composition, exemplified by land use type, is more significant than that of landscape configuration, such as patch shape. Specifically, the PLAND and PD exert the most substantial effects on carbon sequestration and food supply. Meanwhile, ED, SHDI, and LSI have the most pronounced influence on TS-ESF. The direction of this influence varies depending on the spatiotemporal scale. Hence, decision-makers must comprehensively consider the interactions between different landscapes, particularly multifunctional landscapes, to maximize benefits. These findings provide decision-makers with a valuable reference for designing landscape management and creating effective policies to mitigate ecological degradation.

Data availability

All data generated or analysed during this study are included in this published article [and its supplementary information files].

Received: 15 November 2024; Accepted: 18 April 2025

Published online: 06 May 2025

References

- Brander, L. M. et al. Economic values for ecosystem services: A global synthesis and way forward. *Ecosyst. Serv.* **66**, 101606 (2024).
- Gebhardt, S. et al. Supporting stakeholder dialogue on ecosystem service tradeoffs with a simulation tool for land use configuration effects. *Environ. Model. Softw.* **179**, 106097 (2024).
- Monzer Hossain Sarker, M., Gain, A. K., Paul, N. K. & Biswas, S. R. A trait-based approach to quantify ecosystem services delivery potentials in the Sundarbans mangrove forest of Bangladesh. *Ecol. Indic.* **166**, 112390 (2024).
- Chen, M., Liu, W., Lu, D., Chen, H. & Ye, C. Progress of China's new-type urbanization construction since 2014: A preliminary assessment. *Cities* **78**, 180–193 (2018).
- Ji, X. & Chen, B. Assessing the energy-saving effect of urbanization in China based on stochastic impacts by regression on population, affluence and technology (STIRPAT) model. *J. Clean. Prod.* **163**, S306–S314 (2017).
- Li, L., Li, X., Hai, B., Wang, X. & Xu, J. Evolution of rural settlement in an inland nonmetropolitan region of China at a time of rapid urbanisation: The case of Gongyi. *J. Rural. Stud.* **79**, 45–56 (2020).
- Liu, Y., Xiao, H., Lv, Y. & Zhang, N. The effect of new-type urbanization on energy consumption in China: a spatial econometric analysis. *J. Clean. Prod.* **163**, S299–S305 (2017).
- Wang, S., Duan, L., Zhu, Q. & Zhang, Y. Spatial differences of ecological well-being performance in the Poyang lake area at the local level. *Int J Environ Res Public Health* **19**, (2022).
- Wolf-Jacobs, A., Wilson, J. P. & Margulies, E. Promoting self-determination, minimizing green gentrification, and maximizing community benefits in urban forestry expansion: A systematic review. *Urban For. Urban Green.* **84**, 127933 (2023).
- Zhang, R., Chen, S., Gao, L. & Hu, J. Spatiotemporal evolution and impact mechanism of ecological vulnerability in the Guangdong-Hong Kong-Macao Greater Bay Area. *Ecol. Indic.* **157**, 111214 (2023).
- Dawson, L., Elbakidze, M., Angelstam, P. & Gordon, J. Governance and management dynamics of landscape restoration at multiple scales: Learning from successful environmental managers in Sweden. *J. Environ. Manag.* **197**, 24–40 (2017).
- Guo, Y. et al. Multifunctionality can be promoted by increasing agriculture-dominated heterogeneous landscapes in an agro-forestry interlacing zone in northeast China. *Landscape. Urban Plan.* **238**, 104832 (2023).
- Lamothe, K. A. et al. Demand for nonprovisioning ecosystem services as a driver of change in the Canadian boreal zone1. *Environ. Rev.* **27**, 106–123 (2018).
- Peng, J., Ma, J., Du, Y., Zhang, L. & Hu, X. Ecological suitability evaluation for mountainous area development based on conceptual model of landscape structure, function, and dynamics. *Ecol. Indic.* **61**, 500–511 (2016).
- Ren, W., Xu, Y. & Ni, J. Evolution of marine ecology-industry symbiosis patterns and ecological security assessment: New evidence from coastal areas of China. *Ocean Coast. Manag.* **247**, 106939 (2024).
- Tan, P. Y. & Abdul Hamid, A. R. bin. Urban ecological research in Singapore and its relevance to the advancement of urban ecology and sustainability. *Landscape. Urban Plan.* **125**, 271–289 (2014).
- Qiao, E., Reheman, R., Zhou, Z. & Tao, S. Evaluation of landscape ecological security pattern via the “pattern-function-stability” framework in the Guanzhong Plain Urban Agglomeration of China. *Ecol. Indic.* **166**, 112325 (2024).
- Zhang, N., Yuan, R., Jarvie, S. & Zhang, Q. Landscape ecological risk of China's nature reserves declined over the past 30 years. *Ecol. Indic.* **156**, 111155 (2023).
- Huang, F. et al. Exploring the driving factors of trade-offs and synergies among ecological functional zones based on ecosystem service bundles. *Ecol. Indic.* **146**, 109827 (2023).
- Jia, X. et al. The tradeoff and synergy between ecosystem services in the Grain-for-Green areas in Northern Shaanxi, China. *Ecol. Indic.* **43**, 103–113 (2014).
- Wang, K., Gao, J., Liu, C., Zhang, Y. & Wang, C. Understanding the effects of socio-ecological factors on trade-offs and synergies among ecosystem services to support urban sustainable management: A case study of Beijing, China. *Sustain. Cities Soc.* **100**, 105024 (2024).
- Azadi, H., Van Passel, S. & Cools, J. Rapid economic valuation of ecosystem services in man and biosphere reserves in Africa: A review. *Glob. Ecol. Conserv.* **28**, e01697 (2021).
- Puppim de Oliveira, J. A., Bellezoni, R. A., Shih, W. & Bayulkem, B. Innovations in Urban Green and Blue Infrastructure: Tackling local and global challenges in cities. *J. Clean. Prod.* **362**, 132355 (2022).
- Falk, T. et al. Identifying governance challenges in ecosystem services management—Conceptual considerations and comparison of global forest cases. *Ecosyst. Serv.* **32**, 193–203 (2018).
- Montoya, D., Gaba, S., de Mazancourt, C., Bretagnolle, V. & Loreau, M. Reconciling biodiversity conservation, food production and farmers' demand in agricultural landscapes. *Ecol. Modell.* **416**, 108889 (2020).
- Wang, Z., Liu, Y., Li, Y. & Su, Y. Response of ecosystem health to land use changes and landscape patterns in the Karst Mountainous Regions of Southwest China. *Int. J. Environ. Res. Public Health* **19**, (2022).
- Dong, Y., Liu, S., Pei, X. & Wang, Y. Identifying critical landscape patterns for simultaneous provision of multiple ecosystem services—A case study in the central district of Wuhu City, China. *Ecol. Indic.* **158**, 111380 (2024).
- Pirzada, T. et al. Recent advances in biodegradable matrices for active ingredient release in crop protection: Towards attaining sustainability in agriculture. *Curr. Opin. Colloid Interface Sci.* **48**, 121–136 (2020).
- Zhao, J., Wang, S. & Li, J. Study on the spatial-temporal pattern and driving mechanism of tourism eco-security in the Yellow River Basin. *Int. J. Environ. Res. Public Health* **20**, (2023).
- Hu, S. et al. Spatiotemporal dynamics of ecosystem service value determined by land-use changes in the urbanization of Anhui Province, China. *Int. J. Environ. Res. Public Health* **16**, (2019).
- Wang, N., Xu, C. & Kong, F. Value realization and optimization path of forest ecological products-case study from Zhejiang Province, China. *Int. J. Environ. Res. Public Health* **19**, (2022).
- Li, Q., Bao, Y., Wang, Z., Chen, X. & Lin, X. Trade-offs and synergies of ecosystem services in karst multi-mountainous cities. *Ecol. Indic.* **159**, 111637 (2024).
- Yuan, S., Zhu, C., Yang, L. & Xie, F. Responses of ecosystem services to urbanization-induced land use changes in ecologically sensitive suburban areas in Hangzhou, China. *Int. J. Environ. Res. Public Health* **16**, (2019).
- Li, S., Zhao, Y., Xiao, W., Yellishetty, M. & Yang, D. Identifying ecosystem service bundles and the spatiotemporal characteristics of trade-offs and synergies in coal mining areas with a high groundwater table. *Sci. Total Environ.* **807**, 151036 (2022).
- Liu, J. et al. Ecosystem services insights into water resources management in China: A case of Xi'an City. *Int. J. Environ. Res. Public Health* **13**, (2016).
- He, S. et al. Research progress of grassland ecosystem structure and stability and inspiration for improving its service capacity in the karst desertification control. *Plants (Basel)* **12**, (2023).

37. Liu, J. et al. Ecosystem services insights into water resources management in China: A case of Xi'an City. *Int. J. Environ. Res. Public Health.* **13**, (2016).
38. Luo, K. et al. Study on trade-offs and synergies of rural ecosystem services in the Tacheng-Emin Basin, Xinjiang, China: Implications for zoning management of rural ecological functions. *J. Environ. Manag.* **363**, 121411 (2024).
39. Peng, L., Chen, T., Deng, W. & Liu, Y. Exploring ecosystem services trade-offs using the Bayesian belief network model for ecological restoration decision-making: A case study in Guizhou Province, China. *Ecol. Indic.* **135**, 108569 (2022).
40. Costanza, R. et al. Twenty years of ecosystem services: How far have we come and how far do we still need to go?. *Ecosyst. Serv.* **28**, 1–16 (2017).
41. Li, J. & Lei, H. Tracking the spatio-temporal change of planting area of winter wheat-summer maize cropping system in the North China Plain during 2001–2018. *Comput. Electron. Agric.* **187**, 106222 (2021).
42. Bie, Q. et al. Progress toward sustainable development goals and interlinkages between them in Arctic countries. *Heliyon* **9**, e13306 (2023).
43. Dong, X. et al. Entwining ecosystem services, Land Use Change and human well-being by nitrogen flows. *J. Clean. Prod.* **308**, 127442 (2021).
44. Wu, J. et al. Threshold effects and supply-demand ratios should be considered in the mechanisms driving ecosystem services. *Ecol. Indic.* **142**, 109281 (2022).
45. Xu, J., Chen, J., Liu, Y. & Fan, F. Identification of the geographical factors influencing the relationships between ecosystem services in the Belt and Road region from 2010 to 2030. *J. Clean. Prod.* **275**, 124153 (2020).
46. Ocloo, M. D., Huang, X., Fan, M. & Ou, W. Study on the spatial changes in land use and landscape patterns and their effects on ecosystem services in Ghana, West Africa. *Environ. Dev.* **49**, 100947 (2024).
47. Ran, P. et al. The dynamic relationships between landscape structure and ecosystem services: An empirical analysis from the Wuhan metropolitan area, China. *J. Environ. Manag.* **325**, 116575 (2023).
48. Zang, Z. et al. Impact of landscape patterns on ecological vulnerability and ecosystem service values: An empirical analysis of Yancheng Nature Reserve in China. *Ecol. Indic.* **72**, 142–152 (2017).
49. Zhong, M. Impact of landscape patterns on ecosystem services in China: a case study of the central plains urban agglomeration. *Front. Environ. Sci.* **12**, (2024).
50. Huang, J., Xia, Z. & Liu, L. Impacts of landscape configurations on ecosystem services and their trade-offs across different landscape compositions. *Ecosyst. Serv.* **70**, 101666 (2024).
51. Tran, D. X. et al. Quantifying spatial non-stationarity in the relationship between landscape structure and the provision of ecosystem services: An example in the New Zealand hill country. *Sci. Total Environ.* **808**, 152126 (2022).
52. Zheng, L., Wang, Y. & Li, J. Quantifying the spatial impact of landscape fragmentation on habitat quality: A multi-temporal dimensional comparison between the Yangtze River Economic Belt and Yellow River Basin of China. *Land Use Policy* **125**, 106463 (2023).
53. Yuan, L. et al. Decoupling of economic growth and resources-environmental pressure in the Yangtze River Economic Belt, China. *Ecol. Indic.* **153**, 110399 (2023).
54. Chen, Y., Su, X. & Wang, X. Spatial transformation characteristics and conflict measurement of production-living-ecology: Evidence from urban agglomeration of China. *Int. J. Environ. Res. Public Health.* **19**, (2022).
55. Feng, Y., Sun, M., Pan, Y. & Zhang, C. Fostering inclusive green growth in China: Identifying the impact of the regional integration strategy of Yangtze River Economic Belt. *J. Environ. Manag.* **358**, 120952 (2024).
56. Xiang, J., Zhang, W., Song, X. & Li, J. Impacts of precipitation and temperature on changes in the terrestrial ecosystem pattern in the Yangtze River Economic Belt, China. *Int. J. Environ. Res. Public Health.* **16**, (2019).
57. Yang, T., Sun, Y., Li, X. & Li, Q. An ecosystem elasticity perspective of paddy ecosystem sustainability evaluation: The case of China. *J. Clean. Prod.* **295**, 126292 (2021).
58. Grzybowski, M., Furgala-Selezniow, G., Koszalka, J., Kalinowska, J. & Jankun-Woźnicka, M. Correlation between catchment land use/cover and macrophyte assessment of lake ecological status. *Ecol. Indic.* **146**, 109857 (2023).
59. Van Olmen, J. et al. The effect of text message support on diabetes self-management in developing countries—A randomised trial. *J. Clin. Transl. Endocrinol.* **7**, 33–41 (2017).
60. Zhang, J. et al. Climate variability masked greening effects on water yield in the Yangtze River Basin During 2001–2018. *Water Resour. Res.* **58**, e2021WR030382 (2022).
61. Chang, L., Zhao, Z., Jiang, L. & Li, Y. Quantifying the ecosystem services of soda saline-alkali grasslands in Western Jilin Province, NE China. *Int. J. Environ. Res. Public Health.* **19**, (2022).
62. Wu, J., Yang, S. & Zhang, X. Evaluation of the fairness of urban lakes' distribution based on spatialization of population data: A case study of Wuhan Urban Development Zone. *Int. J. Environ. Res. Public Health.* **16**, (2019).
63. Bao, J., Sun, X., Wang, J. & Xie, Y. Quantitative estimates for Lévy driven SDEs with different drifts and applications. *J. Differ. Equ.* **398**, 182–217 (2024).
64. Huang, A. et al. Regional complex system simulation optimization through linking governance and environment performance: A case study of water environmental carrying capacity based on the SDES model. *Environ. Impact Assess. Rev.* **104**, 107356 (2024).
65. Marino, L. & Menozzi, S. Weak well-posedness for a class of degenerate Lévy-driven SDEs with Hölder continuous coefficients. *Stochastic Process. Appl.* **162**, 106–170 (2023).
66. Cabrera Delgado, J. & Bonnel, P. Level of aggregation of zoning and temporal transferability of the gravity distribution model: The case of Lyon. *J. Transp. Geogr.* **51**, 17–26 (2016).
67. Li, R. et al. Will the southward center of gravity migration of population, floor area, and building energy consumption facilitate building carbon emission reduction in China?. *Build. Environ.* **242**, 110576 (2023).
68. Zhang, J. et al. Spatial pattern of technological innovation in the Yangtze River Delta Region and its impact on water pollution. *Int. J. Environ. Res. Public Health.* **19**, (2022).
69. Dou, H. et al. Mapping ecosystem services bundles for analyzing spatial trade-offs in inner Mongolia, China. *J. Clean. Prod.* **256**, 120444 (2020).
70. Lyu, R. et al. Spatial correlations among ecosystem services and their socio-ecological driving factors: A case study in the city belt along the Yellow River in Ningxia, China. *Appl. Geogr.* **108**, 64–73 (2019).
71. Xia, H., Yuan, S. & Prishchepov, A. V. Spatial-temporal heterogeneity of ecosystem service interactions and their social-ecological drivers: Implications for spatial planning and management. *Resour. Conserv. Recycl.* **189**, 106767 (2023).
72. Cheng, M., Huang, B., Kong, L. & Ouyang, Z. Ecosystem spatial changes and driving forces in the Bohai Coastal Zone. *Int. J. Environ. Res. Public Health.* **16**, (2019).
73. Li, W., Kang, J. & Wang, Y. Seasonal changes in ecosystem health and their spatial relationship with landscape structure in China's Loess plateau. *Ecol. Indic.* **163**, 112127 (2024).
74. Tao, Z. et al. Spatiotemporal association of urban park characteristics and physical activity levels based on GTWR: A serial cross-sectional observational study. *J. Urban Manag.* <https://doi.org/10.1016/j.jum.2024.05.004> (2024).
75. Li, J., Zhou, Y., Li, Q., Yi, S. & Peng, L. Exploring the effects of land use changes on the landscape pattern and soil erosion of Western Hubei Province from 2000 to 2020. *Int. J. Environ. Res. Public Health.* **19**, (2022).
76. Liu, L. et al. Remote sensing estimation of regional PM2.5 based on GTWR model—A case study of southwest China. *Environ. Pollut.* **351**, 124057 (2024).

77. Widya, L. K. *et al.* Comparison of spatial modelling approaches on PM(10) and NO(2) concentration variations: A case study in Surabaya City, Indonesia. *Int. J. Environ. Res. Public Health.* **17**, (2020).
78. Ma, X., Zhang, J., Ding, C. & Wang, Y. A geographically and temporally weighted regression model to explore the spatiotemporal influence of built environment on transit ridership. *Comput. Environ. Urban Syst.* **70**, 113–124 (2018).
79. Dong, F., Zhang, S., Long, R., Zhang, X. & Sun, Z. Determinants of haze pollution: An analysis from the perspective of spatiotemporal heterogeneity. *J. Clean. Prod.* **222**, 768–783 (2019).
80. Fu, L. *et al.* Spatiotemporal Heterogeneity and the Key Influencing Factors of PM(2.5) and PM(10) in Heilongjiang, China from 2014 to 2018. *Int. J. Environ. Res. Public Health.* **19**, (2022).
81. Kashki, A., Karami, M., Zandi, R. & Roki, Z. Evaluation of the effect of geographical parameters on the formation of the land surface temperature by applying OLS and GWR, A case study Shiraz City, Iran. *Urban Clim.* **37**, 100832 (2021).
82. Zhu, C. *et al.* Impacts of urbanization and landscape pattern on habitat quality using OLS and GWR models in Hangzhou, China. *Ecol. Indic.* **117**, 106654 (2020).
83. Li, J. *et al.* Study of identification and simulation of ecological zoning through integration of landscape ecological risk and ecosystem service value. *Sustain. Cities Soc.* **107**, 105442 (2024).
84. Pu, X. & Cheng, Q. Unraveling the impacts of multiscale landscape patterns and socioeconomic development on water quality: A case study of the National Sustainable Development Agenda Innovation Demonstration Zone in Lincang City, Southwest China. *J. Hydrol. Reg. Stud.* **51**, 101660 (2024).
85. Hailu, T., Assefa, E. & Zeleke, T. Land use planning implementation and its effect on the ecosystem in Addis Ababa, Ethiopia. *Environ. Challenges* **13**, 100798 (2023).
86. Liu, S., Wang, Z., Wu, W. & Yu, L. Effects of landscape pattern change on ecosystem services and its interactions in karst cities: A case study of Guiyang City in China. *Ecol. Indic.* **145**, 109646 (2022).
87. Wan, D., Liu, J. & Zhao, D. Assessment of carbon storage under different SSP-RCP scenarios in terrestrial ecosystems of Jilin Province, China. *Int. J. Environ. Res. Public Health.* **20**, (2023).
88. Fan, Q., Zheng, Y. & Jia, W. The spatial non-equilibrium and convergence of Chinese grain enterprises' total factor productivity-evidence from China. *Foods.* **11**, (2022).
89. Meng, C. *et al.* Association between multilevel landscape characteristics and rural sustainability: A case study of the water-net region in the Yangtze River Delta, China. *Ecol. Inform.* **82**, 102677 (2024).
90. Wang, Q., Yang, K., Li, L. & Zhu, Y. Assessing the terrain gradient effect of landscape ecological risk in the Dianchi Lake Basin of China using geo-information Tupu method. *Int. J. Environ. Res. Public Health* **19**, (2022).
91. Wang, mWeilin, Yu, H., Tong, X. & Jia, Q. Estimating terrestrial ecosystem carbon storage change in YREB caused by land-use change under SSP-RCPs scenarios. *J. Clean. Prod.* **143205** (2024) <https://doi.org/10.1016/j.jclepro.2024.143205>.
92. Wang, Q., Yang, K., Li, L. & Zhu, Y. Assessing the terrain gradient effect of landscape ecological risk in the Dianchi Lake Basin of China using geo-information Tupu method. *Int. J. Environ. Res. Public Health.* **19**, (2022).
93. Guo, M. *et al.* Developing multiscale landscape planning to mitigate ecological risks: A case study in Nanjing metropolitan area, China. *Environ. Impact Assess. Rev.* **108**, 107601 (2024).
94. Tan, J., Peng, L., Wu, W. & Huang, Q. Mapping the evolution patterns of urbanization, ecosystem service supply-demand, and human well-being: A tree-like landscape perspective. *Ecol. Indic.* **154**, 110591 (2023).
95. Jiang, Y., Ni, H., Ni, Y. & Guo, X. Assessing environmental, social, and governance performance and natural resource management policies in China's dual carbon era for a green economy. *Resour. Policy* **85**, 104050 (2023).
96. Pietrzyk-Kaszyńska, A., Olszańska, A., Rechciński, M., Tusznio, J. & Grodzińska-Jurczak, M. Divergent or convergent? Prioritization and spatial representation of ecosystem services as perceived by conservation professionals and local leaders. *Land Use Policy* **119**, 106193 (2022).
97. Duan, M. *et al.* Effect of present and past landscape structures on the species richness and composition of ground beetles (Coleoptera: Carabidae) and spiders (Araneae) in a dynamic landscape. *Landscape. Urban Plan.* **192**, 103649 (2019).

Acknowledgements

This study was supported by 2021 Guizhou Provincial Philosophy and Social Science Planning Project (21GZQN14).

Author contributions

Y.Y. contributed to the study Evolution or formulation of overall research goals and objectives. Y.Y., executed the tasks of preparing materials, gathering data, and conducting the analysis. The final manuscript was reviewed and approved by all the authors.

Declarations

Competing interests

The authors declare no competing interests.

Additional information

Supplementary Information The online version contains supplementary material available at <https://doi.org/10.1038/s41598-025-99295-z>.

Correspondence and requests for materials should be addressed to Y.Y.

Reprints and permissions information is available at www.nature.com/reprints.

Publisher's note Springer Nature remains neutral with regard to jurisdictional claims in published maps and institutional affiliations.

Open Access This article is licensed under a Creative Commons Attribution-NonCommercial-NoDerivatives 4.0 International License, which permits any non-commercial use, sharing, distribution and reproduction in any medium or format, as long as you give appropriate credit to the original author(s) and the source, provide a link to the Creative Commons licence, and indicate if you modified the licensed material. You do not have permission under this licence to share adapted material derived from this article or parts of it. The images or other third party material in this article are included in the article's Creative Commons licence, unless indicated otherwise in a credit line to the material. If material is not included in the article's Creative Commons licence and your intended use is not permitted by statutory regulation or exceeds the permitted use, you will need to obtain permission directly from the copyright holder. To view a copy of this licence, visit <http://creativecommons.org/licenses/by-nc-nd/4.0/>.

© The Author(s) 2025